ATMOSPHERIC STABILITY IMPACT ON SMALL WIND TURBINE PERFORMANCE IN A COMPLEX TERRAIN

Pedro Alvim de Azevedo Santos
pedroasantos@lepten.ufsc.br

Master Thesis
Mechanical Engineering
Federal University of Santa Catarina

October 2014
Florianópolis-Brazil

UFSC

POSMEC

CNPq
Conselho Nacional de Desenvolvimento Científico e Tecnológico

LEPTEN
Laboratórios de Engenharia de Processos de Conversão e Tecnologia de Energia

Pedro Alvim de Azevedo Santos

IMPACTO DA ESTABILIDADE ATMOSFÉRICA NO DESEMPENHO DE UM PEQUENO AEROGERADOR EM TERRENO COMPLEXO

ATMOSPHERIC STABILITY IMPACT ON SMALL WIND TURBINE PERFORMANCE IN A COMPLEX TERRAIN

Dissertação submetida ao Programa de Pós-Graduação em Engenharia Mecânica da Universidade Federal de Santa Catarina para obtenção do Grau de Mestre em Engenharia Mecânica.
Orientador: Prof. Dr. Júlio César Passos
Coorientador: Prof. Dr. Reinaldo Haas

Florianópolis
2014

Ficha de identificação da obra elaborada pelo autor,
através do Programa de Geração Automática da Biblioteca Universitária da UFSC.

Santos, Pedro Alvim de Azevedo
Impacto da estabilidade atmosférica no desempenho de um pequeno aerogerador em terreno complexo / Pedro Alvim de Azevedo Santos ; orientador, Júlio César Passos ; coorientador, Reinaldo Haas. - Florianópolis, SC, 2014.
129 p.

Dissertação (mestrado) - Universidade Federal de Santa Catarina, Centro Tecnológico. Programa de Pós-Graduação em Engenharia Mecânica.

Inclui referências

1. Engenharia Mecânica. 2. Energia eólica. 3. Pequenos aerogeradores. 4. Turbulência. 5. Micrometeorologia. I. Passos, Júlio César. II. Haas, Reinaldo. III. Universidade Federal de Santa Catarina. Programa de Pós-Graduação em Engenharia Mecânica. IV. Título.

Pedro Alvim de Azevedo Santos

IMPACTO DA ESTABILIDADE ATMOSFÉRICA NO DESEMPENHO DE UM PEQUENO AEROGERADOR EM TERRENO COMPLEXO

ATMOSPHERIC STABILITY IMPACT ON SMALL WIND TURBINE PERFORMANCE IN A COMPLEX TERRAIN

Esta dissertação foi julgada adequada para a obtenção do título de Mestre em Engenharia Mecânica, e aprovada em sua forma final pelo Programa de Pós-Graduação em Engenharia Mecânica da Universidade Federal de Santa Catarina.

Florianópolis, 13 de Outubro de 2014

_____

Prof. Armando Albertazzi Gonçalves Jr., Dr. Eng.
Coordenador do Curso

BANCA EXAMINADORA

_____

Prof. Júlio César Passos, Dr.
Orientador/Presidente

_____

Prof. David Wood, Ph.D.
University of Calgary, Canada

_____

Prof.César José Deschamps, Ph.D.
UFSC

_____

Prof. Juan Pablo Lima de Costa Salazar, Ph.D.
UFSC/Joinville

To my parents, Marcílio and Ligia.

ACKNOWLEDGEMENTS

To Prof. Júlio César Passos, for his guidance and trustful relationship established in the past three years of work.

To Prof. Yoshiaki Sakagami with honorable mention, as a decisive colleague and mentor, who gave the most valuable inputs for this work. To Prof. Reinaldo Haas, for long discussions on academic and technical issues.

To my friends and colleagues of LEPTEN laboratory, for a healthy environment, casual talks and team work. Special thanks to all my undergrad colleagues, for their assistance in data collection and processing.

To André Manoel de Oliveira, for his skillful help in every aspect of installation and test of the experimental setup.

To Tractebel Energia, who sponsored the installed equipment under ANEEL R&D project 0403-0020/2011. Honorable mention to Frederico de Freitas Taves, project engineer that inspired me with valuable technical and non-technical discussions.

To POSMEC graduate program, for the academic support. To CNPq, that sponsored me as a regular master student.

To the entire team of REMA laboratory, that ceased their building structure for the experimental setup deployment. Special thanks to Prof. Henry Corseuil, who encouraged this project since the beginning.

To César Adriano Saupe, who helped me maintain a physical, and thus mental, health.

To the Zen-Buddhist Community of Florianopolis, for the moments of insight and mindfulness.

To all my close friends that shared special moments with me during this period. To Patrícia Backes, with sincere gratefulness.

"*[…] there is no logical way to the discovery of these elemental laws. There is only the way of intuition, which is helped by a feeling for the order lying behind the appearance, and this Einfühlung is developed by experience*."

Albert Einstein, 1933.

ABSTRACT

Small wind turbines in urban environment conditions are usually under high levels of ambient turbulence, influenced by the terrain complexity at the site. The present work evaluates the impact of atmospheric stability on a small wind turbine in a complex terrain, proposing a performance assessment that uses both atmospheric stability and turbulence intensity as criteria. The Obukhov length is chosen as a classification parameter, which is able to quantify the turbulent transport of momentum and heat over the lower portion of the atmospheric boundary layer. The experimental setup used a 2.1 kW wind turbine along with a met mast instrumented with a 3D sonic anemometer, both installed at 19 m next to a two-story building with few nearby obstacles on the university campus. Two years of 10 min wind data show an average turbulence intensity of 32% on site. Therefore, an urban zone environment could be studied with 20 Hz turbulent flux measurements. The selected dataset consists of 4287h of raw data covering a six-month period. Measured power curve following IEC recommendations shows an average performance 14% above the expected manufacturer curve, but with decreasing power output close to the rated wind speed. Values relating power collection increase at low wind speeds with high turbulence levels concur with previous studies. Atmospheric stability was divided into three classes, based on Obukhov length. Stability-dependent power curves were compared with the measured average. Deviations up to 51% in power output were observed between different stability conditions. Above 8 m/s, unstable conditions were predominant and evidenced the declining power tendency, where turbulence intensity was unable to give a consistent outcome. Results reported herein validate a suitable approach for small wind turbines assessment using both physical and statistical parameters as classification criteria. Power surfaces also shows why the proposed assessment better explains the turbine behavior close to rated conditions.

Keywords: Small wind turbines. Turbulence. Micrometeorology. Wind energy.

RESUMO

Quando instalados em zonas urbanas, pequenos aerogeradores estão sujeitos a altos níveis de turbulência atmosférica, influenciados pela elevada complexidade do terreno. O presente trabalho avalia o impacto da estabilidade atmosférica no desempenho de um pequeno aerogerador em um terreno complexo e propõe uma análise de performance com a utilização da estabilidade atmosférica e intensidade de turbulência como parâmetros de análise. O comprimento de Obukhov é escolhido para representar a estabilidade, por ser capaz de quantificar os mecanismos de transporte turbulento de quantidade de movimento e calor ao longo da porção superficial da camada limite atmosférica. A bancada experimental utilizada como estudo de caso é composta de um pequeno aerogerador de 2,1kW de potência e uma torre anemométrica instrumentada com um anemômetro sônico 3D, ambos instalados a 18m ao lado de um prédio no campus da Universidade. Dois anos de dados anemométricos apontam para uma intensidade de turbulência média igual a 32% no local. A base de dados selecionada possui 4287h de dados brutos ao longo de seis meses. A curva de potência medida de acordo com as recomendações da IEC mostrou um desempenho 14% acima da curva do fabricante, mas com queda na potência próximo à velocidade nominal. A correlação entre maior geração em baixas velocidades e altos níveis de turbulência concorda com estudos prévios. Três classes de estabilidade atmosférica foram definidas de acordo com o comprimento de Obukhov. Curvas de potência para cada classe foram então comparadas com a média. Desvios de até 51% foram observados entre diferentes classes de estabilidade. Para velocidades acima de 8 m/s, a condição instável foi predominante e evidenciou a tendência de queda na potência, onde o parâmetro intensidade de turbulência não conseguiu resultados consistentes. Os resultados mostram a consistência da metodologia proposta para análise de desempenho de pequenos aerogeradores com base em parâmetros físicos e estatísticos. Por fim, a construção de superfícies de potência em função da estabilidade e turbulência demonstram bons resultados na descrição da potência extraída próxima à velocidade nominal.

Palavras-chave: Pequenos aerogeradores. Turbulência. Micrometeorologia. Energia eólica.

LIST OF FIGURES

LIST OF TABLES

ACRONYMS AND ABBREVIATIONS

ABL	Atmospheric boundary layer
AEP	Annual energy production
AGL	Above ground level
ANEEL	National Electrical Energy Agency
ASL	Atmospheric surface layer
AWEA	American Wind Energy Association
BWEA	British Wind Energy Association
CF	Capacity Factor
GWEC	Global Wind Energy Council
IEA	International Energy Association
IEC	International Electrotechnical Commission
ISL	Inertial sub-layer
LEPTEN	Laboratory of Energy Technology
MEASNET	Measuring Network of Wind Energy Institutes
MEP	Monthly energy production
MOST	Monin-Obukhov Similarity Theory
REMA	Research Team of Environmental Engineering
RH	Relative humidity
RR	Recovery rate
RSL	Roughness sub-layer
R&D	Research & Development
SWCC	Small Wind Certification Council
SWT	Small wind turbine
TI	Turbulence intensity
UFSC	Federal University of Santa Catarina
WWEA	World Wind Energy Association

LIST OF SYMBOLS

Symbol	Description	Unit
P_{out}	Power output	$[W]$
ρ	Air density	$[kg/m^3]$
c_p	Power coefficient	[-]
A	Rotor swept area	$[m^2]$
U	Horizontal wind speed	$[m/s]$
P_n	Normalized power output	$[W]$
ρ_0	Reference air density (1.225)	$[kg/m^3]$
U_n	Normalized wind speed	$[m/s]$
s_i	Standard uncertainty	$[W]$
u_*	Friction velocity	$[m/s]$
k	Von Karman constant (0.41)	[-]
z	Horizontal height	$[m]$
z_0	Roughness length	$[m]$
$\bar{U}$	Mean wind speed	$[m/s]$
u'	Alongwind fluctuation	$[m/s]$
σ_U	Standard deviation of wind speed	$[m/s]$
OFT	Operation fraction time	[%]
T_U	Unknown operation time	$[h]$
T_N	Non-operational time	$[h]$
T_E	Excluded data time	$[h]$
T_T	Total time	$[h]$
d	Displacement height	$[m]$
z^*	Wake diffusion height	$[m]$
H_{med}	Average obstacle height	$[m]$
v'	Crosswind fluctuation	$[m/s]$
w'	Vertical fluctuation	$[m/s]$

θ'	Temperature fluctuation	$[K]$
f	Coriolis parameter	$[rad/h]$
$\bar{e}$	Mean turbulent kinetic energy	$[m^2/s^2]$
τ	Reynolds stress	$[kg/ms^2]$
$\overline{u'w'}$	Vertical alongwind momentum flux	$[m^2/s^2]$
$\overline{v'w'}$	Vertical crosswind momentum flux	$[m^2/s^2]$
$\overline{w'\theta'}$	Vertical kinematic eddy heat flux	$[mK/s]$
ν	Kinematic viscosity	$[m^2/s]$
θ	Virtual potential temperature	$[K]$
K_m	Eddy viscosity	$[m^2/s]$
K_h	Eddy diffusivity of heat	$[m^2/s]$
l_m	Mixing-length	$[m]$
T_0	Ambient temperature	$[K]$
g	Acceleration due to gravity (9.81)	$[m/s^2]$
H	Vertical sensible heat flux	$[W/m^2]$
c_p	Specific heat at constant pressure	$[J/kgK]$
L	Obukhov length	$[m]$
ϕ_m	Dimensionless wind shear	[-]
ζ	Dimensionless buoyancy parameter	[-]
p_0	Reference pressure (105)	$[Pa]$
p	Atmospheric pressure	$[Pa]$
C_D	Drag coefficient	[-]

SUMMARY

1 INTRODUCTION

Small wind turbines are considered a modern application for distributed generation, acting as a driver towards smart grid systems. According to the World Wind Energy Association (WWEA, 2012) this market has an annual growth of 35%, with more than 300 manufacturers worldwide.

Along with wind energy highlights and promissing applications are the technological challenges, among them a better understanding of the wind resource. Close to the final consumer, small wind grid-tied systems face significant challenges related to the urban environment, characterized by complex terrain, relatively low wind regime and high levels of ambient turbulence.

In order to achieve a sustainable development in wind energy application, studies are seeking tools for more accurate description of the non-linear aspects involved in the atmospheric boundary layer (ABL) dynamics (LANGE; FOCKEN, 2006). Within this region wind profile is influenced by turbulence, shear, among other factors. Exponential and logarithm functions are used to describe the wind profile, but if not properly corrected are valid in restrict atmospheric conditions (ARYA, 2001). Therefore, wind profile variations under distinct atmospheric conditions can provide more reliable wind power assessment.

The importance of wind profile correction according to atmospheric stability was already known (STULL, 1988), but gained the attention of the wind energy industry more recently, with the deployment of wind turbines with large swept areas, therefore, more sensitive to wind profile. When exposed to a larger and a higher portion of the ABL, the power output will be better predicted with an accurate description of the wind profile (WHARTON; LUNDQUIST, 2012).

In the context of the urban environment, a higher terrain complexity is observed, combining topography and high surface roughness effects, with more challenges for wind flow description, mainly because of its site-specific nature. Small wind roadmaps point out the lack of understanding of turbulence and directional variability in urban environment, along with wakes, eddies and separation zones, as main barriers for reliable small wind applications (SMITH et al., 2012).

1.1 RESEARCH PROBLEM

The present work aims to perform an experimental study to characterize atmospheric stability in an urban environment site and correlate the results with power collection of a small wind turbine.

With an adequate stability parameter, it will be possible to infer variations in the wind profile and characterize power collection deviations for different wind regimes and atmospheric conditions. The Monin-Obukhov Similarity Theory (MOST) will be invoked for the calculation of the stability parameter. MOST can be understood as a semiempirical structure which provides a quantitative and physical parameter of turbulence (ARYA, 2001).

The results of this work aim to evaluate the hypothesis of atmospheric stability influence on small wind turbine power collection and raise the relevant parameters to assess it. On the road to a better description of urban wind flow, corrections considering atmospheric stability and wind profile variations could then improve small wind turbine (SWT) design, performance assessment, safety and operation.

Therefore, the primary challenge of this work is to create an experimental setup capable of measuring and correlating atmospheric stability conditions with SWT power collection in an urban environment. In essence, the following research question can lead the current study: What is the impact of atmospheric stability on the performance of a small wind turbine and how to assess it?

1.2 OBJECTIVES

In order to answer the research question, the primary objective is:

- Assess the impact of atmospheric stability on the performance of a small wind turbine in a complex terrain.

The main objective unfolds in specific goals:

- Understand the role of atmospheric stability in kinetic energy extraction by a wind turbine;
- Design and construct an experimental setup with a small wind turbine and met mast to collect data of wind, power generation and turbulent fluxes;
- Characterize atmospheric stability, turbulence intensity and wind turbine performance parameters;
- Correlate the atmospheric stability parameter and turbulence intensity with wind turbine power collection;
- Develop a procedure for power performance assessment using atmospheric stability applied to small wind turbines.

1.3 RELEVANCE AND CONTRIBUTIONS

Atmospheric stability effects on wind turbine performance is already a common research topic among large wind farms (WAGNER; COURTNEY, 2010; WHARTON; LUNDQUIST, 2012). The selection of a stability parameter based on MOST is also applied in the cited studies, but this kind of approach has yet to be applied for small wind turbine applications.

Within the urban environment, turbulence is generated not only at the large scale, but also locally by shear and wake-inducing obstacles. Recent papers studied the influence of turbulence on small wind turbine performance, both with experimental measurements (LUBITZ, 2014) and numerical simulations (SUNDERLAND et al., 2013). These studies found difficulties in the use of the statistical parameter of turbulence intensity to address the turbulence influence on small wind turbines.

Hence, the research problem can be considered up to date and with relevance for a better description of urban environmental flow, once it plans to go beyond turbulence intensity, with the use of a physical parameter as metric for turbulence. An approach already consolidated in large wind turbine studies will be used to evidence the behavior of SWT in urban areas. The results aim to be recognized as contributions for:

- Establishing favorable and adverse atmospheric conditions for small wind generation in complex terrain;
- Formulating better tools for wind resource assessment in the urban environment;
- Presenting a methodology for SWT power performance assessment based on atmospheric stability and turbulence intensity.

1.4 CONSTRAINTS

A case study will be designed to verify the hypothesis of atmospheric stability influence on the performance of a small wind turbine. This case study consists in an experimental setup with a SWT and a meteorological mast close to a building. Therefore, all the results are considered site-dependent. The analysis period is also restrained by the experiment deployment date and performance.

Considering the terrain complexity involved, some experimental constraints will appear. In order to fulfill the MOST's hypothesis and requirements for turbulent flux measurements, collected data will be filtered with dedicated software.

The focus of the present work is on the influence of flow conditions on power collection. Small wind turbine control aspects aren't analyzed

in detail, and malfunctioning events are also filtered. Furthermore, the wind profile isn't calculated or measured, owing to the lack of instruments.

1.5 OUTLINE

The structure of this work is organized around the presented research problem, seeking to display a precise relation between the micrometeorological tools and wind energy knowledge applied to the experimental setup and studied dataset.

Chapter 2 presents some aspects related with wind energy and small wind turbines, as well as the theoretical basis for atmospheric stability analysis. Chapter 3 summarizes the experimental setup constructed for this work, with equipment specifications and measured variables, as well as the selected dataset used for power performance analysis, including filtering procedures.

Chapter 4 shows the main results involving atmospheric stability effects on small wind turbine power curves, with the average regime of atmospheric stability on the site. Chapter 5 discusses some concluding points of the presented results, proposing some topics for further studies and possible uses for the experimental setup. The Appendix presents the published papers related with this study, as well as extra details and measurements of the experimental setup. Attachments present the SWT project documentation.

2 THEORETICAL BACKGROUND

A great range of subjects are involved with the research problem, but two are chosen to lead towards the results and conclusions of this work, wind energy and micrometeorology. Specific aspects of each topic, which were applied in the methodology, are highlighted herein with the citation of others references being indicated when needed.

Concerning wind energy, specialized reports from international agencies and institutions (GWEC, 2012; IEA, 2014) present market data, as well as discussions dealing with the current state and world perspectives. For the Brazilian national scenario, the work of Damas (2013) is suggested. Santos (2011) presents a physical understanding of wind's kinetic energy extraction by a wind turbine, applying the basic concepts of mass, energy and momentum conservation within a control volume.

Micrometeorology can be interpreted as the part of meteorology study mainly concerned with local processes. Foken and Nappo (2008) highlighted the application of micrometeorology aspects as part of the wind energy research field.

2.1 WIND ENERGY

Great importance is being given to wind power applications worldwide, with moderate perspectives pointing to a share of 6% in the global generation by 2020 (GWEC, 2012). In Brazil, the scenario is also inspiring, with 63% growth in 2011 and 2GW installed in the country (EPE, 2013). Another interesting point are the Brazilian prices for wind in the energy auctions, where wind farms reached $ 50/MWh in 2011, the cheapest renewable energy in Brazil at that time (DAMAS, 2013).

The small wind turbines (SWT) market also has fast-growing behavior. Although not close to large wind market numbers and still concentrated in stand-alone applications in China, this technology can be a driver towards more distributed generation systems. Equipment prices for small wind applications reached $ 3,000/kW in United States during 2011 (WWEA, 2012). Economic viability, however, is achieved not only with small kW-installed prices, but with a reliable estimation of annual energy production and proper understanding of local wind regime.

Santos *et. al.* (2011) present different scenarios of economic viability for small wind turbines in urban environments, pointing the importance of reliable estimation for annual energy production (AEP).

For large wind turbines, Damas et al. (2012) spotted major deviations between planned and observed capacity factors in Brazilian wind farms. Therefore, wind resource is predictable but needs to be carefully studied for each case.

2.1.1 Power performance

The power produced by a wind turbine can be related with the available power in the wind multiplied by a power coefficient, $\dot{c_p}$ (Eq. 2.1). From equation 2.1, it's easy to notice that power generation is a function of the cube of velocity at nacelle height.

$$P_{out} = \frac{1}{2}\rho \dot{c_p} A U^3 \tag{2.1}$$

The previous discussion about the proper description of wind temporal and spatial distribution is, in fact, relevant. It's worth noting the existence of a physical limit for wind kinetic energy extraction, known as the Betz-Joukowsky limit, equals to 59,3% (SANTOS, 2011; WOOD, 2011). Consequently, wind energy can be understood as kinetic energy conversion into electricity, considering a stochastic source in space and time with an equipment with aerodynamic, mechanical and electrical losses.

The International Electrotechnical Commission (IEC) is currently responsible for the international standard covering power performance measurements, entitled IEC 61400-12-1. This standard primarily defines the procedure for power curve measurement and calculation. Three important aspects are detailed below: data normalization, method of bins, and uncertainty bars (IEC, 2005). Some additional requirements are also defined by the Measuring Network of Wind Energy Institutes (MEASNET, 2009a).

In order to compare power curves from different measurement sites, air density is chosen a parameter for normalization. Hence, the normalized power curve is corrected for the reference air density, ρ_0, taken as 1.225 kg/m^3, with the relations in equations 2.2 and 2.3,

$$P_n = P_{10min}\frac{\rho_0}{\rho_{10min}}, \tag{2.2}$$

$$U_n = U_{10min}\left(\frac{\rho_0}{\rho_{10min}}\right)^{1/3}, \tag{2.3}$$

where all measured power and wind velocity data is corrected with the reference value, resulting in the normalized measurement. IEC 61400-12-1 uses 10 min average to construct the power curve, but for small wind turbines (Annex H) pre-processed data shall also be stored with 1-min duration (IEC, 2005).

Power curve is determined by grouping measured data in bins. The method of bins defined by IEC is composed by the average of normalized speed and power over intervals of 0.5 m/s, centered on multiples of 0.5 m/s. The range of valid bins should cover 1 m/s below the cut-in wind speed to 1.5 times the wind speed at 85% of the rated power.

Each bin has an associated uncertainty. The category A standard uncertainty of power is used herein, defined by the standard deviation of power over the normalized averaged value divided by the square root of the number of data sets in each bin, expressed in equation 2.4,

$$s_i = \frac{1}{\sqrt{N_i}} \sqrt{\frac{1}{N_i - 1} \sum_{j=1}^{N_i} \left[\left(\frac{1}{N_i} \sum_{j=1}^{N_i} P_{n,i,j} \right) - P_{n,i,j} \right]^2} \tag{2.4}$$

where s_i is the category A uncertainty of power of bin i, $N_i$is the number of 1 min data sets in bin i and $P_{n,i,j}$ is the normalized power output of dataset j in bin i.

Figure 1 presents the power curve of a three-blade upwind horizontal axis small wind turbine with active yaw drive and stall control. The starting point of power production is set as a cut-in wind speed, around 3 m/s. The rated wind speed specifies turbine's performance. In the presented case, the advertised power is 100kW at a rated speed of 12 m/s, even though the measured curve does not reach the claimed power output. The cut-out wind speed, usually set at 25 m/s, is when the turbine shuts down for safety reasons.

Two distinct regions can be identified in a typical power curve: the "ankle" region, characterized by a close to cubic increase in power production, around 6 m/s, and the "knee" region, around the rated speed, where the control system shifts away from tracking a maximum power coefficient. Wood (2011) draws attention to the importance of an efficient power control, so that the turbine does not extract more energy that can be absorbed by the generator and at the same time accounts for unsteady behavior, indicating high turbulence levels, when operating close to the rated wind speed.

Figure 1 – AGW 100C/24 and NPS 100-24 power curve.

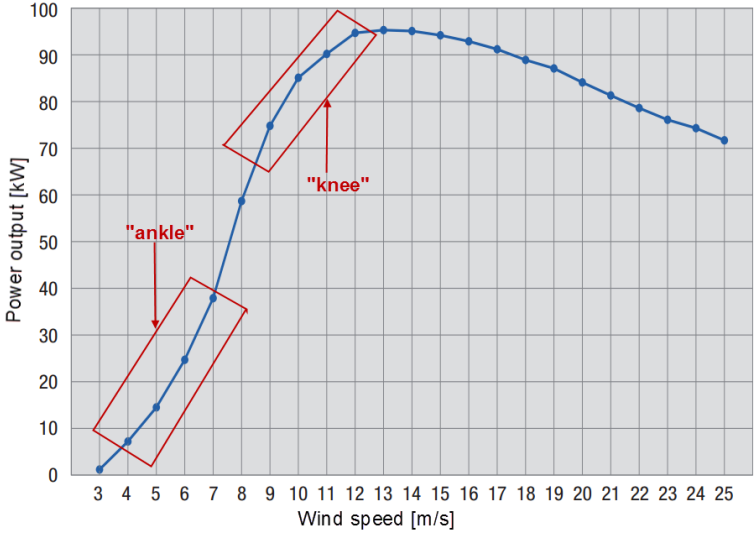

Source: WEG and Northern Power Systems.

2.1.2 Wind resource

Hau (2006) reminds us that wind resource maps, satellite wind data (e.g. EUMETSAT) or global numerical models (e.g. Reanalysis) are useful but not sufficient to account for microscale effects. According to the recommendations of IEC 61400-12-1 and MEASNET (2009b), wind resource assessment starts with a measurement campaign on the site, in order to capture the local wind regime at different heights. With this wind data one can perform a horizontal extrapolation for distinct positions, using software with microscale models such as *WAsP*®, *WindPRO*® and *WindSim*®. For each position, however, a vertical extrapolation is also needed, in order to capture the velocity at nacelle height or the entire profile over the turbine's swept area. These softwares also have different strategies and parameterizations. *Meteodyn WT*® and *WAsP CFD*®, for example, already account for atmospheric stability effects on vertical extrapolation.

The common practice in wind energy industry is to consider the average velocity gradient ($\partial U/\partial z$) only dependent on the height above the ground (z) and the friction velocity (u_*), defined as $u_* = \left(\tau_w/\rho\right)^{1/2}$.

This hypothesis will be presented in detail in Section 2.2, resulting in the well-known logarithmic wind profile (ARYA, 2001), in Eq. 2.5,

$$U(z) = \frac{u_*}{\kappa} \ln\left(\frac{z}{z_0}\right) \tag{2.5}$$

where z_0 represents the surface roughness and κ is the von Karman constant. Tables for commonly used values of surface roughness are showed in Santos (2011), Hau (2006) and Arya (2001). For engineering purposes, the ratio u_*/κ is graphicaly determined based on the measured profile, since high frequency data would be needed for friction velocity calculation (BURTON et al., 2001). The profile of equation 2.5 is only valid for neutrally stratified conditions, which occurs around 10% of the time (ARYA, 2001), as detailed in Section 2.2. This is another reason for the discussion about the necessity of wind profile correction in the industry.

Along with the spatial distribution, wind speed is rarely steady and also varies in time. The Weibull function is commonly used to describe the frequency distribution of wind (HENNESSEY, 1977). Turbulence intensity (TI) is the chosen parameter by IEC to evaluate velocity fluctuations with the available instruments in the wind energy industry. To present the definition of TI, first consider the Reynolds averaging hypothesis, based on Figure 2.

Figure 2 – Measured wind vector at 20 Hz.

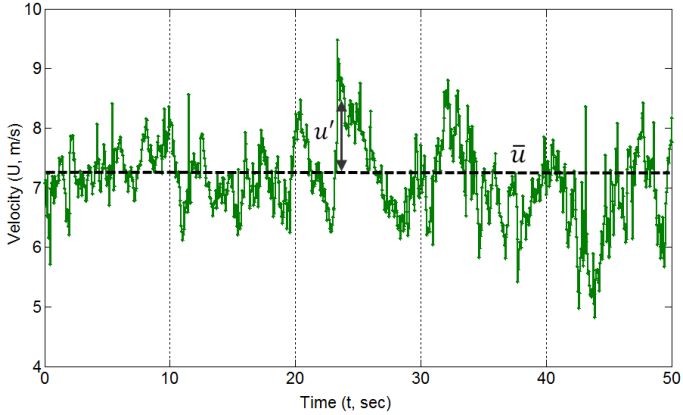

Considering a statistically stationary turbulent flow, at any time t, we can decompose the velocity vector, U, in a mean value, $\bar{U}$, and a fluctuation, u', so that,

$$U(t) = \overline{U} + u' \tag{2.6}$$

From figure 2, we can note that for the presented hypothesis, the mean fluctuation value for a given interval is zero, or $\overline{u'} = 0$. The turbulence intensity can then be defined as,

$$TI = \frac{1}{\overline{U}}\left[\frac{1}{T}\int_0^T u'^2 dt\right]^{1/2} = \frac{\sqrt{\overline{u'^2}}}{\overline{U}} = \frac{\sigma_U}{\overline{U}} \tag{2.7}$$

where T is the averaging interval, and $\sigma_u$is the standard deviation of velocity U. For TI calculation, a period T = 10 min is used, following the IEC standard. In practice, this parameter is used to quantify turbulence, varying from 10% at low roughness site to 20% or more in urban environment (WOOD, 2011).

Equation 2.7 shows the statistical nature of the TI parameter, as a ratio between standard deviation and average. Authors that already used TI to evaluate SWT performance comment about some issues, strongly supported in the fact that urban areas have relatively low wind speeds and consequently unreal values of TI, once significant standard deviations dominate the results (SUNDERLAND et al., 2013).

Elliot and Cadogan (1990) presented a relation between the TI parameter and power performance by inserting the Reynolds average decomposition, Eq. 2.6, in the power collection equation, Eq. 2.1. Using TI definition, Eq. 2.7, the average cubic wind speed is,

$$\overline{U^3} = \overline{(\overline{U} + u')^3} = \overline{U}^3\left(1 + 3\frac{\overline{u'^2}}{\overline{U}^2}\right) = \overline{U}^3(1 + 3TI^2) \tag{2.8}$$

Hence, the average power output, $\bar{P}$, can be expressed as,

$$\overline{P_{out}} = \frac{1}{2}\rho c_p A\overline{U^3} = \frac{1}{2}\rho c_p A\overline{U}^3(1 + 3TI^2) \tag{2.9}$$

This relation indicates a direct quadratic dependence between power and TI, which is not true at the knee region, where the power output starts to decrease. The non-linear behavior of the power curve can be accounted with an expansion of $\overline{P_{out}}$ in the Taylor series (GOTTSCHALL; PEINKE, 2008).

Even with limitations, a comparison between the IEC-based measured power curve and the estimation of Eq. 2.9 will be performed for a given TI intensity in order to assess the influence of TI parameter in the ankle region. When mean power curves are simulated, higher TI

levels show an increased performance for velocities below the rated wind speed and lower power output close to rated conditions (WAGNER; COURTNEY, 2010).

2.1.3 Small wind turbines

Small wind turbines are classified under distinct criteria by each wind energy association or institution. Most commonly known, IEC 61400-2 defines the threshold of 200 m^2 for the SWT rotor swept area, with a maximum rated power of about 50 kW. The American Wind Energy Association (AWEA) and the Small Wind Certification Council (SWCC) consider equipment up to 100 kW of rated capacity as small or medium wind turbines. The Britsh Wind Energy Association (BWEA) also has a medium wind class, with turbines up to 1,000 m^2 of swept area and rated power up to 500 kW.

Independent certification schemes, such as SWCC and BWEA, are useful and relevant, being able to filter and select the most reliable equipment. With a large number of manufacturers, also come plenty of under tested turbines with high potential for damage the industry reputation.

The International Energy Agency (IEA) also released a report for "*Technical recommendations for small wind turbine consumer labelling*," in the context of Task 27, with the objective to summarize standards and apply for the world small wind market. Task 27 is now dedicated to evaluating "*Small wind turbines in high turbulence sites*," aiming for best practices of Built-environment Wind Turbines (BWT) design and testing. The present work aims to give some insights into the same topic, with a large database of turbulent wind data captured at high frequency (20 Hz).

Unlike large wind turbines, SWT technology has a wide variation in types and sizes. Vertical axis, multi-blade and even two-blade technology (e.g. Gaia Wind) are used in SWT applications. However, with the lack of refined control strategies, a lower efficiency is usually observed when compared to large turbines. Therefore, a SWT efficiency of 20% can be considered high (WOOD, 2011).

An important point to be stated is that each turbine has its particular duty. SWTs with low rated power, as in figure 3a, would probably have a successful use in stand-alone applications but could be a disaster in a built-environment. On the other hand, medium turbines, as in figure 3b, can contribute to a small community in a grid-tied distributed system.

Figure 3 – 160W stand-alone turbines (a); 100kW grid-tied tubine (b).

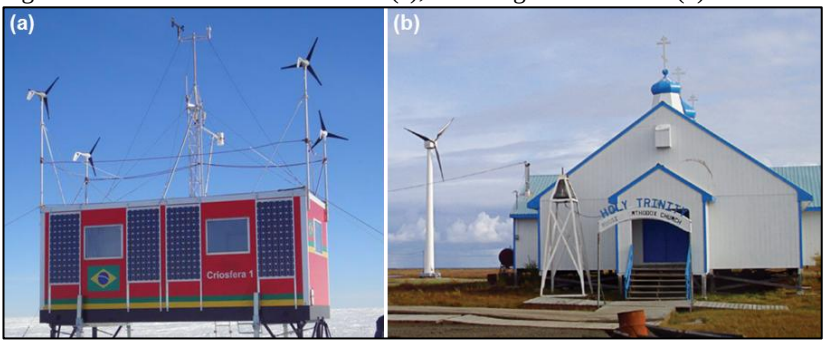

Source: Brazilian Institute for Space Research (a); Northern Power Systems (b)

Small wind turbine applications in urban environment consider that production is close to the final consumer, who also has connection to the grid. In Brazil, the National Electrical Energy Agency released in 2012 the regulatory framework for renewable energy distributed generation systems with up to 1MW of installed capacity (ANEEL, 2012a, 2012b). Smith et al. (2012) comment about different cases of successful SWT application under government compensation schemes.

Figure 4 – Distributed generation net metering scheme.

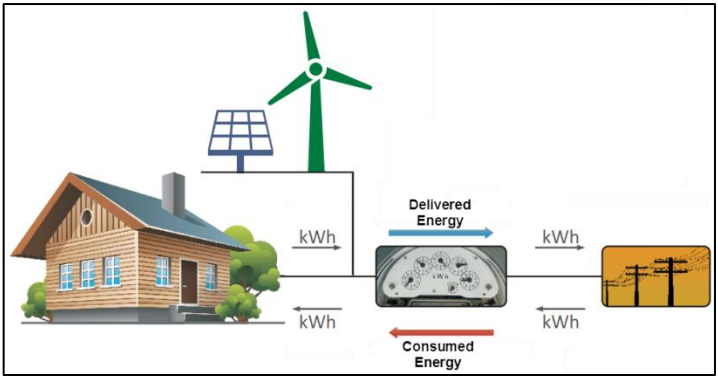

Source: Adapted from ANEEL (2014).

Net metering was chosen as the Brazilian first compensation scheme, illustrated in figure 4. In this case, the net balance of generated and consumed power is evaluated by a bi-directional energy meter. For a positive balance, namely more generated than consumed power, the credit is registered by the local distributor, who grants a discount in the

upcoming bill. It's worth noting the absence of a feed-in tariff; hence the generated power is "sold" at the local energy price for that household.

Each local distributor can establish their connection requirements. In Santa Catarina state, where the experimental setup is held, the only condition for connections up to 300 kVA is to have the bi-directional meter and an atmospheric discharge protection system after the inverter (CELESC, 2013). With this national scenario, the appearance of small and medium wind turbines in Brazil will probably increase in the next few years.

Specific for small wind turbines, the IEC 61400-2 standard discusses not only design requirements, but approaches procedures for duration tests. According to this standard, during a six-month period the SWT should present at least 90% of operational fraction time (Eq. 2.10), *OFT*, over 2500h of power production in wind of any velocity.

$$OFT = \frac{T_T - T_N - T_U - T_E}{T_T - T_U - T_E} \times 100\% \quad (2.10)$$

From the total operation time, T_T, is deduced events of non-operational behavior, T_N, unknown turbine status, T_U and excluded data events, T_E. At least 250h of operation should happen above 10.2 m/s ($1.2V_{ave}$) and 25h above 15.3 m/s ($1.8V_{ave}$), considering a IEC 61400-2 Class II turbine (V_{ave}=8.5 m/s). No major failure or significant power degradation at comparable wind speeds should be noticed (IEC, 2013). These requirements will be verified in the presented experimental setup of this work.

2.1.4 Urban environment

A critical step for a small wind distributed generation system is the proper equipment location. Buildings and other high surface roughness obstacles can generate wakes and undesired local turbulence. Figure 5 presents the rule of thumb for an undisturbed region around obstacles (FOKEN; NAPPO, 2008). Stankovic, Campbell and Harries (2009) give practical examples of different types of small and medium wind turbines applications and SWT positioning close to buildings.

Numerical simulations have been made in order to evaluate the potential of built-mounted wind turbines. Such studies (LEDO; KOSASIH; COOPER, 2011) have provided compelling insights regarding the effects of turbine positioning, as well as predictions for near-obstacle wind profiles. Commercial softwares like *UrbaWind*® aim to provide wind resource assessment in urban zones, for various

applications such as natural ventilation, thermal comfort, heat islands and SWT performance potential.

Figure 5 – SWT positioning options around obstacles.

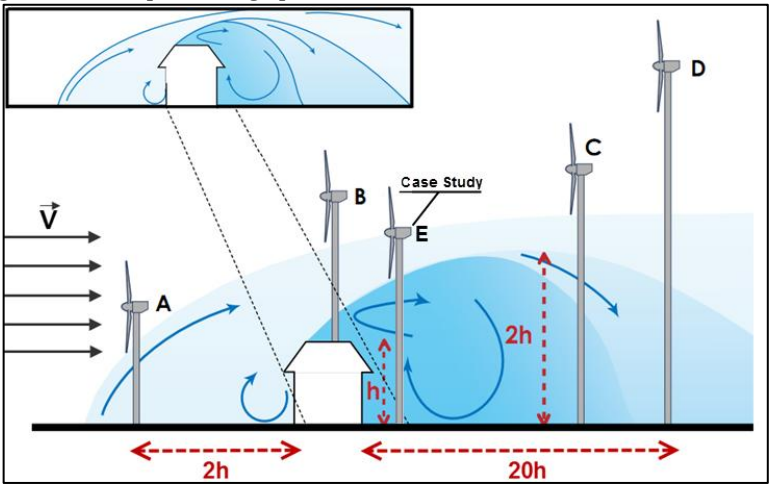

Source: Adapted from Stankovic, Campbell and Harries (2009)

Unlike rural environments, in urban zones the best possible location is not always viable, and the tradeoff between AEP and final cost has to be considered (MERTENS, 2006). In figure 5, positions A to D show some possible locations within an undisturbed flow region. The present work aims to simulate an intermediate position (E in fig. 5), where the SWT is installed nearby a building at about two times its height. The main objective is to escape from the cavity and wake regions that form behind the obstacle (ARYA, 2001), but at the same time capture high turbulence levels.

The Warwick Wind Trials study (ENCRAFT, 2008) is frequently cited as an example of some unsuccessful applications, with measured discrepancies between the expected and generated power production, both in rural and urban environment. The majority of books and experts concur that any homeowner or industry interested in small wind application should exercise a degree of caution. If the minimum amount of information on the local wind resource is not available, or in the case of doubt about performance and safety issues, do not proceed without further advice.

Experimental studies have also been carried to correlate SWT power performance measurements with ambient turbulence. TI is commonly used as a correlation parameter. Lubitz (2014) reported

experimental results for the variation in the power output based on turbulence intensity (TI), measuring a 2% decrease in the power output for low TI (<0.14) between 4 m/s and 7 m/s. Results are less consistent for high TI (>0.18) values. Sunderland et al. (2013) performed power curve simulations for different turbulence intensity levels, considering a neutrally stratified atmosphere. All of the above studies agree that, for lower wind speeds, high turbulence levels can improve the SWT power collection in urban environments. In contrast, turbulence tends to reduce the performance at rated wind speed.

Since obstacles have a remarkable influence on local turbulence production and therefore on meteorological measurements, its worth noting that the log law profile (Eq. 2.5) is not entirely valid under urban environments, as well as mountain regions and forest canopies (MERTENS, 2006). Foken and Nappo (2008) show that for rural environments with dense vegetation, the wind profile should be corrected with a zero-plane displacement height, *d*, given by

$$U(z) = \frac{u_*}{\kappa} \ln\left(\frac{z-d}{z_0}\right), \tag{2.11}$$

that can be understand as the effective zero wind speed height, so that $U(z_0 + d) = 0$. Figure 6 presents a sketch of an air-flow model over the urban canopy, where the observed profile (blue line) is quite different from the log-law from Eq. 2.11 (red dashed line). Mertens (2006) points that the extrapolation of equation 2.11 has to account the presence of a roughness sub-layer (RSL) within the canopy, dominated by turbulence eddies, stagnation points as well as wakes and recirculation zones.

Figure 6 – Urban average horizontal velocity profile.

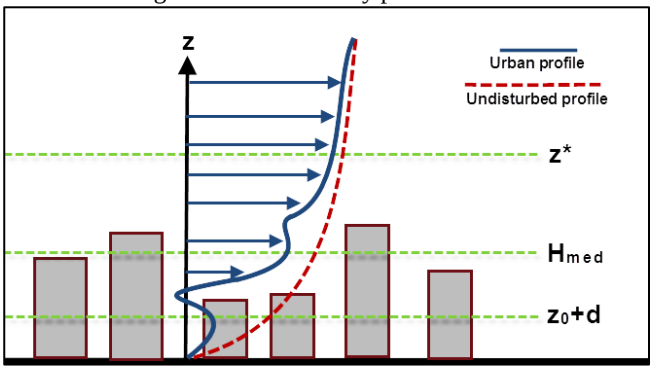

The RSL is considered between the average building height, H_{med}, and the wake diffusion height, z^*, where the logarithmic profile is no longer applicable, thus $H_{med} < z < z^*$ (SUNDERLAND et al., 2013). Above the RSL we have an inertial sub-layer (ISL), $z > z^*$, where the effects of individual surface types are blended and turbulent fluxes can be considered constant with height, therefore reaching the behavior of the atmospheric surface layer (ASL), as described in Section 2.2.

Sunderland et al. (2013) take $z^* = 2H_{med}$ in order to place a sonic anemometer for high frequency measurements. The same approach is going to be conduced in the present work, with the objective of measuring turbulent fluxes that can be further correlated with a similarity theory.

Urban environment and other regions with complex terrain and high surface roughness all have different aspects of nonhomogeneous boundary layers. Arya (2001) and Oke (1987) describe aspects related to this inhomogeneity and urban boundary layer effects, respectively. The focus is on a physical approach for the turbulence and SWT performance link. A significant effect to be studied is the thermal stratification of the atmosphere and the relation with turbulence production and atmospheric stability, detailed next.

2.2 MICROMETEOROLOGY

The characterization of atmospheric stability, and wind profile variations, starts with the comprehension of the ABL's non-linear aspects. Micrometeorology deals with the local ABL aspects both in space (1 km) and time (1 hour) (ARYA, 2001). It is inside the ABL that the turbulence and shear effects from the interaction with the surface will be relevant (STULL, 1988). Figure 7 shows a cross-section from which the ABL can be seen as being the 20% bottom part of the troposphere.

Figure 7 – Troposphere vertical cross section.

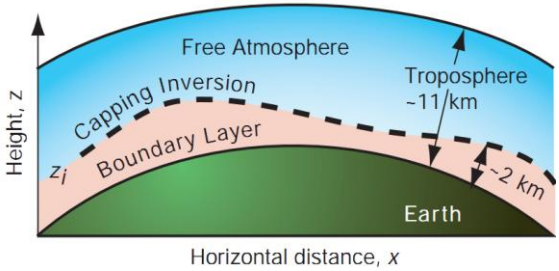

Source: Wallace and Hobbs (2006).

The bottom 10% of the ABL is called atmospheric surface layer (ASL), where turbulent fluxes and shear are significantly influenced by topography and roughness elements (STULL, 1988). It is within the ASL region that the presented measurements are obtained. Monin and Obukhov (1954) consider that the ASL could vary between 50m and 250m above the ground.

2.2.1 Portrait of turbulence

Turbulence is ubiquitous within the ABL, conferring its non-linear behavior (WALLACE; HOBBS, 2006). In fact, most atmospheric flows have all the essential characteristics of a turbulent flow, which goes beyond a merely quasi-random and chaotic movement, with a laminar behavior restricted to viscous sub-layers over smooth surfaces (ARYA, 2001).

An atmospheric wind profile has an effective diffusivity of momentum, heat and mass over its length, being a three dimensional and rotational flow with vorticity as well as multiple scales of motion. These fundamental characteristics underline the notion of a turbulent flow, with a superposition of different sized eddies – swirls of motion – that interact in a non-linear form to continuously dissipate the kinetic energy supplied by the mean flow. This idea of an energy cascade, flowing from the larger scale until the smaller turbulent eddies was suggested by Lewis Richardson (1922) in a famous parody,

> Big whorls have little whorls,
> Which feed on their velocity;
> And little whorls have lesser whorls,
> And so on to viscosity.

Richardson's whorls are our definition of eddies hereinafter. The smaller eddies are created from a breakdown process from larger eddies, along with a partial energy transfer and dissipation between scales. Arya (2001) points out that largest eddies are produced by mean flow shear and thermal convection (buoyancy effects). This notion of the production mechanisms of turbulence, together with eddy diffusivity of momentum and heat will be essential to quantify turbulence and, therefore, atmospheric stability further.

The statistical notion of Reynolds average (1895) was already presented in equation 2.6 along with figure 2. Equation 2.12 presents the incompressible Navier-Stokes equations, in a rotating frame of reference

tied to the earth's surface (STULL, 1988). In the next equations, it's worth noting the use of Einstein notation, where: $u_1 = u'$ is the alongwind fluctuation, $u_2 = v'$ the crosswind component and $u_3 = w'$ is the vertical velocity fluctuation.

$$\frac{\partial U_i}{\partial t} + U_j \frac{\partial U_i}{\partial x_j} = -g\delta_{i3} + f U_j \varepsilon_{ij3} - \frac{1}{\rho}\frac{\partial P}{\partial x_i} + \nu \frac{\partial^2 U_i}{\partial {x_j}^2} \qquad (2.12)$$

$$I \qquad II \qquad III \qquad IV \qquad V \qquad VI$$

The storage of momentum (Term I) is influenced by the advection (Term II), gravitational effect (Term III), earth's rotation (Term IV), pressure-gradient forces (Term V) and viscous stress (Term VI). The Coriolis force, Term (IV), is described by the parameter $f = 2\omega \sin\phi$, where $\omega = \frac{2\pi}{24} rad/h$ and ϕ is the local latitude.

The conservation of mass with constant density can be stated as an incompressibility condition, in equation 2.13. We can readily apply the average over eq. 2.13 and verify in equation 2.14 that both mean and fluctuating velocities satisfy the incompressible continuity equation as if they were independent flows (MATHIEU; SCOTT, 2000).

$$\frac{\partial U_i}{\partial x_i} = \frac{\partial (\overline{U}_i - u_i)}{\partial x_i} = \frac{\partial \overline{U}_i}{\partial x_i} - \frac{\partial u_i}{\partial x_i} = 0 \qquad (2.13)$$

$$\frac{\overline{\partial U_\iota}}{\partial x_\iota} = \frac{\overline{\partial (\overline{U}_\iota - u_\iota)}}{\partial x_\iota} = \frac{\partial \overline{U}_i}{\partial x_i} - \frac{\partial \overline{u}_i}{\partial x_i} = 0 \;\therefore\; \frac{\partial \overline{U}_i}{\partial x_i} = 0 \;\therefore\; \frac{\partial u_i}{\partial x_i} = 0 \qquad (2.14)$$

Once we understand the averaging procedure, with the use of relations presented in 2.14, equation 2.12 can be expressed as,

$$\frac{\partial \overline{U}_i}{\partial t} + \overline{U}_j \frac{\partial \overline{U}_i}{\partial x_j} = -g\delta_{i3} + f\overline{U}_j \varepsilon_{ij3} + \frac{1}{\rho}\frac{\partial}{\partial x_j}\left\{-\bar{P}\delta_{ij} + \mu\left(\frac{\partial \overline{U}_i}{\partial x_j} + \frac{\partial \overline{U}_j}{\partial x_i}\right) - \rho\overline{u_\iota u_j}\right\}; \qquad (2.15)$$

known as the Reynolds-averaged Navier-Stokes (RANS) equations, the Reynolds stress tensor, $-\rho\overline{u_\iota u_j}$, can be identified. This nonlinear symmetric tensor introduces a coupling between the mean and turbulent parts of the flow, therefore having to be solved or parameterized in order to determine the mean velocity field.

The turbulent transport expressed by the Reynolds tensor can not be neglected; on the contrary, it is the dominant component over molecular transport. Within the ABL, molecular transport dominates over turbulent transport only over in the lowest few centimeters of air above the ground, forming a region that Stull (1988) called interfacial sublayer.

Let's describe a transport equation for the double correlation $\overline{u_i u_j}$, but presented as the turbulent kinetic energy (TKE) budget equation, since $TKE = \bar{e} = 0.5\overline{u_i u_i} = 0.5(\overline{u'^2} + \overline{v'^2} + \overline{w'^2})$. Subtracting (2.12) from (2.15), multiplying by u_j and summing the equation with exchanged index give the $\overline{u_i u_j}$ variance budget equation. TKE budget can be expressed dividing the variance budget by 2 with $i = j$,

$$\underset{I}{\frac{\partial \bar{e}}{\partial t}} + \underset{II}{\bar{U}_j \frac{\partial \bar{e}}{\partial x_j}} = \underset{III}{+g\frac{(\overline{u_i \theta'})}{\bar{\theta}}\delta_{i3}} \underset{IV}{- \overline{u_i u_j}\frac{\partial \bar{U}_i}{\partial x_j}} \underset{V}{- \frac{\partial(\overline{u_j e})}{\partial x_j}} \underset{VI}{- \overline{\frac{u_i}{\rho}\frac{\partial p}{\partial x_i}}} \underset{VII}{- \varepsilon} \quad (2.16)$$

TKE is considered one of the most important variables for the turbulence study. Equation 2.16 describes the evolution of this physical parameter for turbulence intensity (Term I), evidencing the physical processes that generate turbulence within the ABL. Term II relates the advection of TKE by the mean flow. It´s worth noting the absence of the Coriolis term that became zero for the turbulent part, showing no influence of earth's rotation in turbulence generation.

Term III can be a production or consumption component. The buoyancy influence depends on the heat flux $\overline{w'\theta'}$, that can thermally produce TKE if positive (at daytime over land) or consume TKE if negative (at night over land). Term IV is the mechanical production component, since momentum flux $\overline{u_i u_j}$ is usually lost downward to the ground, therefore a positive term arises representing shear production.

Term V can be interpreted as TKE turbulent transport. Term VI is a redistribution term caused by pressure perturbations. Term VII is the viscous dissipation of TKE, which converts energy into heat. Therefore, we can see that turbulence is a dissipative process because Term VII is always negative, since $\varepsilon = \nu\overline{\left(\frac{\partial u_i}{\partial x_j}\right)^2}$.

The physical description of turbulence sheds light into the production and dissipative mechanisms involved in the energy cascade concept. The relation between thermal production or consumption and shear production will define how momentum and heat are transported, hence affecting the wind profile.

Equation 2.16 also shows that an additional triple correlation $\overline{u_i u_i u_j}$ arises (Term V), which will also need to be described in order to solve the mean flow. If a transport equation for the triple correlation is derived, a fourth correlation will appear. Hence, the number of unknowns in the RANS equations is always larger than the actual number of equations. The necessity to solve the additional tensor components is called the closure problem (ARYA, 2001). In fact, the full statistical description and solution of turbulence is one of the unsolved problems of classical physics (STULL, 1988).

2.2.2 Closure Assumptions

In order to solve equation 2.15, a finite number of equations are used along with closure assumptions. Therefore, the unknown turbulent fluctuation terms have to be parameterized as a function of measured quantities, as well as empirical parameters. A first order closure, for example, would use equation 2.15 and parameterize the Reynolds tensor (ARYA, 2001). Higher-order closures, which are not the scope of this work, are discussed by Stull (1988).

The older and more widely used first-order approach is to assume a hypothetical analogy between molecular and turbulent transport. By lending the gist of Newton's law of molecular viscosity, J. Boussinesq proposed in 1877 that the turbulent shear stress in the direction of the flow may be expressed as $\tau = \rho K_m \left(\partial U / \partial z\right)$, where K_m is called the eddy viscosity. A gradient transport theory based on eddy viscosity can be extended from this assumption, in order to parameterize the vertical momentum fluxes and also sensible heat flux, here with an analogy from Fourier's law. Therefore, we can express,

$$\overline{u'w'} = -K_m \, \partial U / \partial z \; ; \; \overline{w'\Theta'} = -K_h \, \partial \Theta / \partial z \qquad (2.17)$$

where K_h can be understood as a eddy diffusivity of heat. It is worth mentioning that, unlike molecular viscosity, the eddy diffusivity parameters, K_h and K_m, are flow properties.

With the goal of describing the eddy viscosity in terms of flow parameters, in 1925 L. Prandtl extended the molecular analogy and described a hypothetical mechanism for turbulent mixing, the mixing-length hypothesis. With a parallel with the kinetic theory of gases, Prandtl hypothesized that turbulent fluxes (eddies) breakaway from their flow layer and travel a certain distance, a free path length, called mixing-length, l_m.

Figure 8 – Wind profile with turbulent fluctuations.

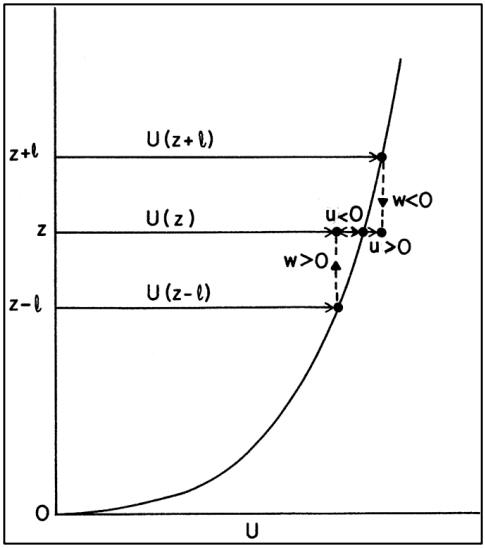

Source: Arya (2001)

A longitudinal velocity at z, $U(z)$, receives eddies from above and below. The lower eddy ($w' > 0, u' < 0$) transport momentum and generates negative fluctuations. The higher eddy ($w' < 0, u' > 0$) gives rise to positive fluctuations. Note that $\overline{u'w'} < 0$, as expected. Therefore, the average fluctuation for U is,

$$\left\|\overline{u'}\right\| = \frac{1}{2}(\Delta U_{z+l} + \Delta U_{z-l}) = l_m \left\| {}^{\partial U}/_{\partial z} \right\| \qquad (2.18)$$

With the natural assumption that turbulent fluctuations have the same order of magnitude, we can extend 2.18 for $\left\|\overline{w'}\right\|$ and express the vertical momentum flux $\overline{u'w'}$ as well as determine an algrebric relation for K_m correlating the mixing length hypothesis with the gradient transport theory, hence,

$$\overline{u'w'} = -l_m^2 \left\| {}^{\partial U}/_{\partial z} \right\| {}^{\partial U}/_{\partial z} \quad \therefore \quad K_m = l_m^2 \left\| {}^{\partial U}/_{\partial z} \right\| \qquad (2.19)$$

The mixing-length hypothesis considers that turbulence is only mechanically generated by a local wind shear, thus ignoring transport as well as thermal effects. Considering a neutral surface layer, Arya (2001) shows that the eddy viscosity can be parameterized as $K_m = kzu_*$, where k is Von Karman's constant and the friction velocity can be

approximated to $u_* \cong \sqrt{-\overline{u'w'}}$. Inserting the eddy viscosity parameterization in eq. 2.19, we can easily deduce the logarithmic profile previously described in eq. 2.5,

$$u_*^2 = kzu_* \, {\partial U}/{\partial z} \;\; \therefore \;\; \frac{\partial U}{\partial z} = \frac{u_*}{kz} \;\; \therefore U(z) = \frac{u_*}{k} ln\left(\frac{z}{z_0}\right) \qquad (2.20)$$

This logarithmic profile is evaluated inside the ASL, which can go from 50 to 250m above the ground. It is within this region that Coriolis force is ignored and turbulent fluxes are considered constant with height (MONIN; OBUKHOV, 1954). Arya (2001) points out that the presented neutrally-stratified profile is an exception rather than a rule in the lower atmosphere. Therefore, an extension of these assumptions become necessary, in order to consider the component related to thermal production or consumption of TKE.

2.2.3 Monin-Obukhov Similarity Theory

In the real atmosphere, however, the turbulent exchange of heat along the ABL generates a thermal stratification of the atmosphere, which directly impacts the wind profile. The Monin-Obukhov Similarity Theory (MOST) provides a suitable extrapolation with a quantitative description of turbulence structure in a thermally stratified surface layer. It is considered a semiempirical framework since it corrects the wind profile with empirical relations as a function of a dimensionless parametrization.

The basic similarity hypothesis, proposed by Monin and Obukhov (1954) considers that in a horizontally homogeneous surface layer, the mean flow and turbulence fluctuations depend on four independent variables: the height above the surface z, the surface drag ${\tau}/{\rho} = u_*^2$, the surface kinematic sensible heat flux ${H}/{\rho c_p}$ and the buoyancy effect ${g}/{T_0}$. This relation can be understood as a straight extension from the neutral stratified case, which ignores the last two variables related with thermal inhomogenities within the atmosphere, i.e.,

$$\frac{\partial U}{\partial z} = f\left(z, u_*, {H}/{\rho c_p}, {g}/{T_0}\right) \qquad (2.21)$$

Assumptions considered for the relationship presented in 2.21 are that the flow is horizontally homogeneous, quasistationary, turbulent fluxes of momentum and heat are constant with height, molecular

exchanges are insignificant over turbulent transport, and rotational effects can be ignored inside the ASL (ARYA, 2001). With Buckingham's theorem, a single dimensionless parameter can be derived to express the proposed relation. The combination traditionally chosen is the buoyancy parameter $\zeta = {}^{z}/_{L}$ where,

$$L = -\frac{u_*^3}{\left[k\left({}^{g}/_{T_0}\right)\left({}^{H}/_{\rho c_p}\right)\right]} \tag{2.22}$$

is known as the Obukhov length. Like other stability parameters, Eq. 2.22 can be understood as the ratio between mechanically generated turbulence by thermally produced/consumed turbulence.

Therefore, the Obukhov length module, $|L|$, is described by Arya (2001) as the height above the ground under which friction effects are always important. Extreme values for L tend to indicate a neutrally stratified surface layer, where neither thermal nor mechanical turbulent components are dominant. In contrast to turbulence intensity, the Obukhov length is considered a physical stability parameter, for the sake of turbulent eddies assessment, and it is going to be used to assess the atmospheric stability in this work.

The friction velocity parameter, u_*, has a direct relation with vertical momentum fluxes. Considering MOST hypothesis, u_* can be calculated as,

$$u_* = \left(\overline{u'w'}^2 + \overline{v'w'}^2\right)^{1/4} \tag{2.23}$$

The sensible heat flux H quantifies the vertical turbulent transport of heat (Eq. 2.24). Like the friction velocity, it is also considered constant with height within the ASL, according to MOST.

$$H = \rho c_p \overline{w'\Theta'} \tag{2.24}$$

It is important to mention that the kinematic vertical heat flux $\overline{w'\Theta'}$ determines the sign of the Obukhov length and, therefore, the resulting stability, as further explained. With the calculation of momentum and thermal turbulent fluxes an individual wind profile correction with the stability parameter for each predominant condition can be done (LANGE; FOCKEN, 2006).

With the dimensionless parameter $\zeta = {}^{z}/_{L}$, a relation for the corrected wind profile can be stated as,

$$\frac{kz}{u_*}\frac{\partial U}{\partial z} = \phi_m(\zeta) = \phi_m\left({}^{z}/_{L}\right) \tag{2.25}$$

where the similarity function, ϕ_m, has to be experimentally determined from field data. Micrometeorological experiments have measured turbulent fluxes and developed estimations for this universal similarity function, in order to correct the wind profile. Arya (2001) discusses some experiments and proposed empirical functions for wind profile correction in non-neutral situations. One of the most cited experiments is the *Kansas Field Program*, performed in 1968, which resulted in a generally accepted forms for ϕ_m (Eq. 2.26), with constants corrected in further studies (FOKEN, 2006).

$$\phi_m\left(\frac{z}{L}\right) = \begin{cases} \dfrac{1}{\left(1 - 19.3\frac{z}{L}\right)^{0.25}}, for\ \dfrac{z}{L} < 0 (unstable) \\ 1, \quad for\ \dfrac{z}{L} = 0 (neutral) \\ \left(1 + 6\dfrac{z}{L}\right) \quad , for\ \dfrac{z}{L} > 0 (stable) \end{cases} \tag{2.26}$$

The present work aims to assess and analyze the Obukhov length stability parameter, in order to correlate with power collection measurements. Flux measurements are performed to determine atmospheric stability, but wind profile parameterization with similarity functions is not the main purpose of this work.

2.2.4 Atmospheric stability

Atmospheric stability is related to buoyant convection (static) and wind shear production (dynamic) (STULL, 1988), that will determine the transition and permanence in a turbulent state. Unstable flows become and remain turbulent, in turn a stable atmosphere tends to become laminar. Hence, this concept is basically about a state of equilibrium (WALLACE; HOBBS, 2006). This is why the ratio between mechanically produced and thermally produced/consumed TKE is used as a stability parameter.

Local definitions of static stability are determined by the local lapse rate, i.e., the potential of a parcel of air to climb upward or to descend in the atmosphere. Stull (1988) points out that the measurement of the lapse rate alone is insufficient to determine static stability. A nonlocal description, based on the kinematic vertical heat flux $\overline{w'\theta'}$ can be

applied. With a net upward heat flux ($\overline{w'\theta'}$>0) unstable conditions, with low wind shear, are observed. On the other hand, a stable environment is characterized by high wind shear and a negative sensible heat flux ($\overline{w'\theta'}$<0).

As stated above, when these thermal inhomogeneities become relevant, buoyancy mechanisms of production and consumption tend to affect the wind shear profile. Figure 9 shows the diurnal cycle of a measured wind profile.

Figure 9 – Diurnal cycle of measured wind speeds at different heights

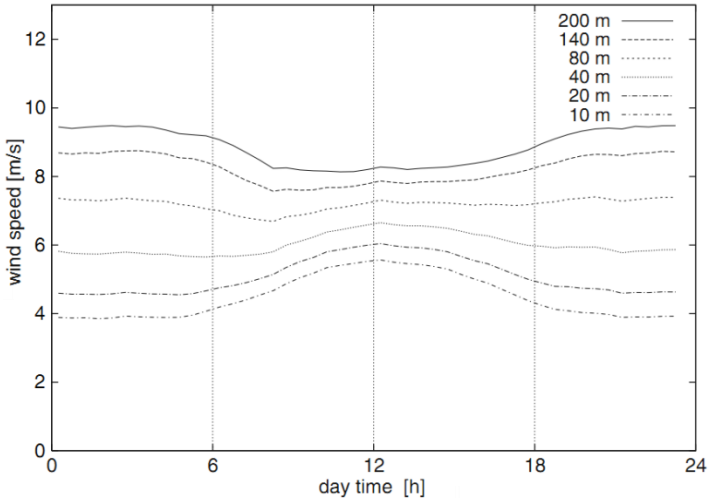

Source: Lange and Focken (2006).

An unstable atmosphere, also called convective, can be observed during daytime over land, where the heated ground surface generates a net upward heat flux. This active momentum transport mechanism with convection cells increases the mixing within the ASL, hence reducing the wind shear, as showed in Fig. 9 between 9h and 17h.

At night, the situation is inverted. The net downward heat flux generates a thermally stratified condition that increases the wind shear, as observed in Fig. 9 between 18h and 6h.

Returning to Obukhov length, Eq. 2.22, it's worth noting that for moderate values of u_*, unstable conditions ($\overline{w'\theta'} > 0$) are identified by negative values of L, in turn stable conditions ($\overline{w'\theta'} < 0$) give rise to positive values for this parameter. Wharton and Lundquist (2010) performed measurements to assess the impact of atmospheric stability over the performance of large wind turbines. Their atmospheric stability

classification (Table 1) used Obukhov length (L), turbulence intensity (TI) and turbulent kinetic energy (TKE). The present work applies a similar stability classification as the aforementioned study.

Table 1 – Stability classification for different parameters.

Stability	L [m]	TI [%]	TKE [m^2/s^2]
Strongly stable	0 < L < 50	TI < 8	TKE < 0,4
Stable	50 < L < 200	8 < TI < 10	0,4 < TKE < 0,6
Neutral	(L > 200) or (L < -300)	10 < TI < 20	0,6 < TKE < 1
Convective	-300 < L < -15	20 < TI < 30	1 < TKE < 1,4
Strongly convective	-15 < L < 0	TI > 30	TKE > 1,4

Source: Wharton and Lundquist (2010)

With more precise measurements, recent studies quantified the influence of stability on wind profile and wind turbine production. The Wharton and Lundquist (2012) wind farm study reported strong seasonal and diurnal variations in the wind profile, which increases energy production during stable conditions and reduces the output for unstable profiles. This study also constructed specific power curves for each stability condition.

Wagner et al. (2011) propose that power collection calculation can be performed with a rotor average wind speed, due to the enormous influence of wind shear in large wind turbines. Sathe, Gryning and Peña (2011) also present a stability classification based on flux measurements and show the impact on the wind profile.

This work seeks to perform an analogy of the cited studies applied to SWT power performance. Thus, an atmospheric stability assessment will be performed, based on flux measurements and Obukhov length, in order to correlate the results with SWT power collection data. So for this study, the L parameter calculation requires the selection of a flux measurement technique.

2.2.5 Eddy Covariance

With the use of a 3D ultrasonic anemometer, latitudinal, longitudinal and vertical wind speeds, as well as high frequency fluctuations from the mean (u', v', w', θ'), can provide detailed information on the eddy structures. Therefore, the selected method for this study is known as eddy covariance. Considered one of the most accurate and defensible methods for flux measurements, it directly

calculates the momentum, heat and other gas transport covariances (AUBINET; VESALA; PAPALE, 2012).

Since this application is focused on turbulent diffusion of momentum and heat, the vertical perturbations of velocity and heat are measured at 20 Hz frequency. The calculated turbulent fluxes will represent the transport eddies in the ASL. Therefore, the Obukhov length in Eq. 2.22 is rewritten in terms of measured variables as,

$$L = -\frac{\left(\overline{u'w'}^2 + \overline{v'w'}^2\right)^{\frac{3}{4}} T_a \left(p_0/p\right)^{0.286}}{\kappa g \overline{w'\theta_v'}} [m] \quad (2.27)$$

where $\overline{u'w'}$ and $\overline{v'w'}$ ($m^2\ s^{-2}$) are the kinematic vertical momentum fluxes, k is the von Karman constant (0.41) and g is acceleration due to gravity (9.81 $m\ s^{-2}$). $\overline{w'\theta_v'}$ ($m\ K\ s^{-1}$) is the kinematic vertical sensible heat flux. The virtual potential temperature (θ, K) is evaluated based on the ambient temperature (T_a, K) with an atmospheric pressure (p, Pa) reference correction (p_0=10^5 Pa).

An averaging period is chosen in order to consider all eddy sizes within its measurement. A 60min averaging time is usually taken for tall forest canopies (LEE; MASSMAN; LAW, 2004). However, to perform this average over an hour, transient effects for each perturbation have to be minimized. Figure 10 illustrates this issue.

The block average method only subtracts the mean flow from the signal in the chosen period. A linear detrending, however, finds the line of best fit over that period. Therefore, for a transient regime as showed in Fig. 10, fluctuations around the average are better represented with the second technique. Lee, Massman and Law (2004) present further methods, such as running mean and exponential running mean.

Figure 10 –High-frequency detrending methods

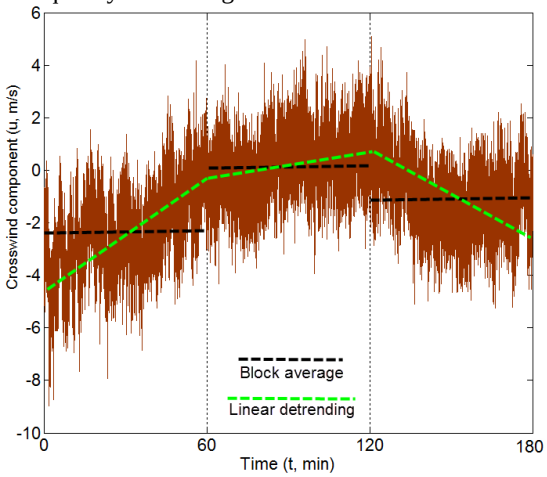

Another source of errors in flux estimation is the possibility of a misalignment of the sonic anemometer with local wind streamlines, caused by a tilted instrument or flow deviations by the terrain. Rotation methods are applied to correct velocity fluctuations and stress components. Double rotation technique rotates the coordinate system to nullify the average crosswind ($\overline{v'}$) and vertical fluctuation ($\overline{w'}$) components. Triple rotation also finds a new angle to compensate the crosswind stress covariance ($\overline{v'w'}$). Rotation effects can introduce 10% to 25% of systematic error in the measurements (LEE; MASSMAN; LAW, 2004).

Foken (2008) alerts for the use of double and triple rotation methods in tall forest canopies and other types of complex terrain, since the zero vertical fluctuation plane does not necessarily match with the mean flow streamline. Lee, Massman and Law (2004) suggest the planar fitting method, that considers the vertical component (w') as a linear combination of the alongwind (u') and crosswind (v') fluctuations, fitting a plane to the resulting average vertical component ($\overline{w'}$).

When dealing with high frequency measurements, a statistical treatment also needs to be performed, since unreal fluctuation values and suspicious trends are not uncommon. An important statistical filter for the present application involves the representative angle of attack of average fluxes reaching the anemometer, α. With obstacle influence this type of occurrence needs to be identified and removed (Fig. 11).

Figure 11 – Angle of attack representation.

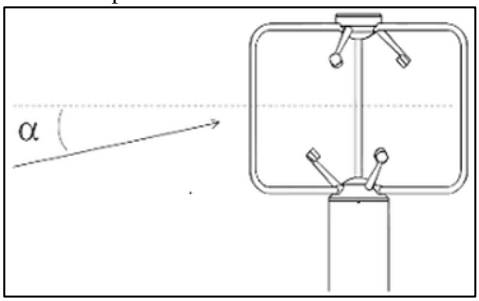

Source: LI-COR (2013)

Spike removal aims to exclude outranged short-term data from the analysis, which can cause systematic errors of 2% and random errors up to 11% (on 30min average) (LEE; MASSMAN; LAW, 2004). On rainy days or in similar events, the optical sonic path can be obstructed, causing values outside the control limits. Therefore, a drop-out test aims to filter this kind of occurrence. Other important statistical filters are related to values out of the absolute limits and discontinuities.

One of the objectives of flux post-treatment is to validate the measured fluxes with MOST basic assumptions. A key eddy covariance assumption is a horizontal and uniform terrain, so that average fluctuations can be considered zero and flow convergence as well as divergence affects are negligible. In a terrain with high surface roughness, steady-state situations can be spotted in order to reproduce a fair wind regime and reduce uncertainties. New techniques and adaptations in the classical eddy covariance are under development, treating situations such as tall forest canopies and hills, as well as urban areas (LEE; MASSMAN; LAW, 2004).

Vickers and Mahrt (1997) discuss the quasi-stationary condition that needs to be satisfied, and how to filter crosswind and alongwind components to account only for steady flow patterns. Their presented procedure evaluates the systematic variations in both wind components that constitute the horizontal wind. With the quadratic combinations of such components, a threshold can be specified, therefore, classifying unsteady horizontal wind regimes.

Aubinet, Vesala and Papale (2012) compiled a practical guide that emphasizes the requirements and constraints for commissioning a flux measurement tower. The present experimental setup lies in a suburban area, hence not meeting all the requirements for flux estimation. Rather

than meet all the best practices, the objective is a rough estimation of turbulent fluxes in order to assess atmospheric stability.

Sonic data, measured at 20 Hz, were post-processed using EddyPro® open source software (LI-COR, 2013). It consists in a processing package for raw eddy covariance data, with all of the filtering and analysis aspects discussed in this topic. Mainly focused on biosphere and atmospheric fluxes of CO_2, H_2O and CH_4, it has many other tools for environmental micrometeorological applications.

3 MATERIALS AND METHODS

The present work is part of an ANEEL R&D project in partnership with the company Tractebel Energia, from GDF Suez. With the additional objective to study distributed generation and small wind applications, the experimental setup with a SWT and a 10m meteorological mast began at the university campus in March 2012.

A project for this case study was developed with our team of the Laboratory of Energy Technology (LEPTEN) at Federal University of Santa Catarina (UFSC). A 2.1kW SWT and first-class measurement sensors were purchased, along with a 3D ultrasonic anemometer. The meteorological mast was installed in November of 2012, and the SWT was commissioned and started operation in January of 2013.

Figure 12 shows the experimental setup, which is located inside the univeristy farm, at Campus Sul da Ilha in the city of Florianópolis (27°41'1.02"S, 48°32'43.46"W). Both the SWT and meteorological mast are installed close to the building of a research team in Environmental Engineering (REMA).

Figure 12 –Wind Energy Experimental Setup at UFSC

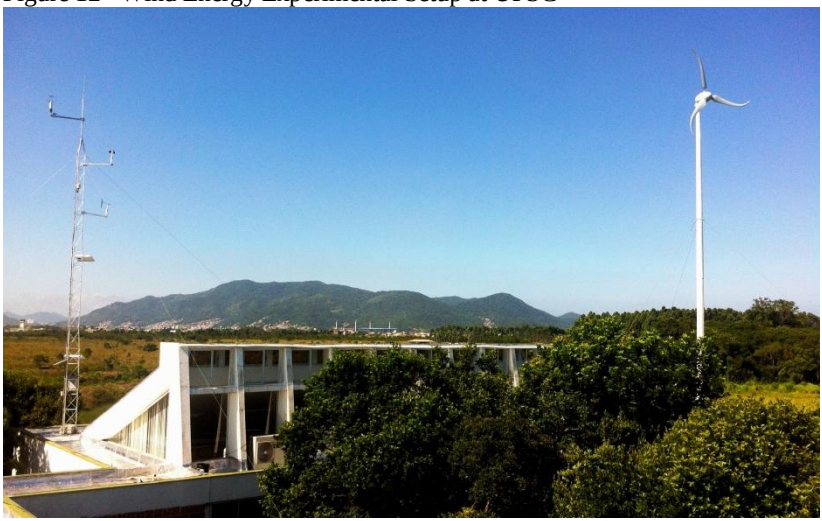

3.1 SMALL WIND TURBINE

Based on previous studies of Santos et al.(2011), Skystream 3.7 was the selected SWT to compose the experimental setup. This 3-blade horizontal axis wind turbine has a great range of applications across the

world, with more than 8000 units operating by 2006. The equipment has also been tested by different organizations, with available database and certification reports according to IEC 61400-12-1.

Southwest Windpower was the company that developed and was selling the equipment until 2013, when it was acquired by Xzeres Wind Corporation. Based on the test report from WINDTEST GmbH (2009), Skystream 3.7 has SWCC's certification since 2012, current under number SWCC-10-20. Table 2 presents the product specifications.

Table 2 – Installed SWT specifications

Model:	Skystream 3.7
Serial Number:	KK-2011-0238
Power form:	240 VAC, 1-phase, 60 Hz
Hub Height:	18.9m
Rotor diameter:	3.72 m
Swept area:	10.87 m^2
Cut-in wind speed:	3.0 m/s
Max Power Output:	2.4 kW
Rated power:	2.1 kW
Rated wind speed:	11 m/s
Downwind with stall regulation	
Passive yaw control	

The installation was performed in January 2013 and operation began, but soon some pitfalls were noticed. A structural resonance was observed in the 19m monopole tower during the first weeks, almost reaching a critical point of natural frequency. Hence, in March of 2013 a new tower, with thicker walls, was installed in the same layout. Oscillations were reduced, but momentum was still being transferred to the building, with potential structural damage. Noise was also a complaint of the researchers and students inside the building.

Therefore, in December 2013 the tower was removed from the original location and placed at a distance of 3m from the building. The new cylindrical reinforced concrete foundation followed a certified project (Attachment A), with 1.2m in diameter and 2.1m in depth. Guy wires were installed in the monopole tower with two stages, to reduce oscillations.

In the end, the final layout consisted in a 19m "guyed" monopole tower. A theodolite was used for tower alignment, using the guy wires as regulation marks. After three months, realignment had to be performed, indicating the tower was under excessive vibration. This

practical experience of tower relocation showed some of the many challenges involving built-integrated small wind applications.

The SWT is directly connected in the building main panel, following the electrical diagram, also in Attachment A. Since there was already a bi-directional kilowatt-hour meter connected to the utility grid, a grid-tied application that meet all the CELESC requirements for a distributed generation system was installed. All the produced energy is supplied for the University laboratories. Figure 13 shows the certified power and cp curves that will be used as reference data (WINDTEST, 2009).

Figure 13 – Certified Skystream 3.7 power and Cp curves

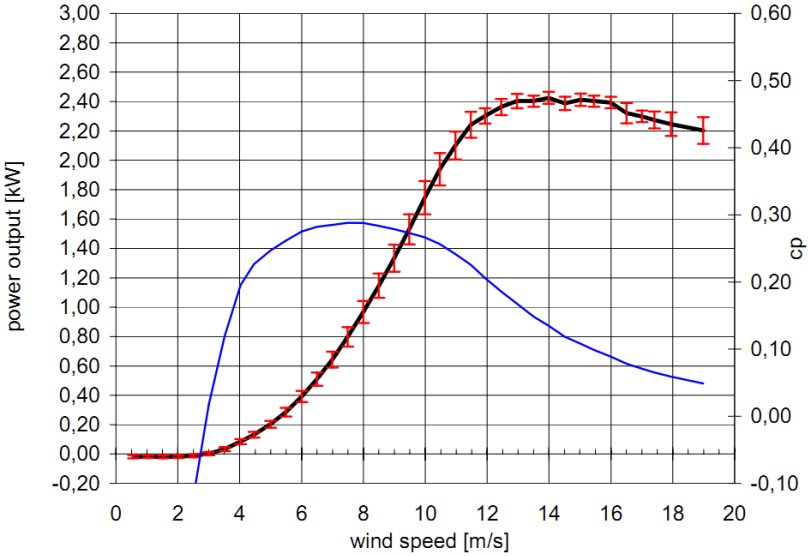

Source: Windtest (2009)

In order to measure an IEC-based power curve for the presented case study it was installed a power transducer. Therefore, a dedicated energy meter and the safety switch of Attachment B were not considered. In turn, this calibrated transducer is connected to the meteorological mast, so that all power collection data can be acquired and recorded at 1 Hz frequency, along with other measurements

The operation regime of Skystream 3.7 wind turbine could be monitored by the Skyview software. Variables such as voltage, frequency, RPM, power output, among others, were available, but the software showed a weak connection and could not be trusted for a long-

time assessment. Therefore, the installed power transducer replaced the manufacturer software for power output measurements, with a higher accuracy ($\pm 0.5\%$) and the possibility for real-time monitoring and data storage when connected to the CR1000 data logger.

3.2 METEOROLOGICAL MAST

For the hub height wind measurements, a meteorological mast was installed on the top of the same building. The tower was place at a distance of 20 m from the SWT, facing the prevailing wind, at a height of 18 m_{agl} (above ground level).

The met mast is operating since November 18th, 2012. For configuration and testing issues, the 3D sonic anemometer was installed in March 15th, 2013. The main occurrences are registered in the experiment's logbook (Appendix A1). Since the SWT started a proper operation regime with a new tower in December of 2013, this month will be the starting period of analysis in the selected dataset (Section 4.2).

The met tower consists of a 3D sonic velocity and sonic temperature sensor at the top, one level of wind speed and direction, along with pressure, temperature and humidity measurements. Solar panels, summing 60 Wp, charge a battery setup designed for 14 days without sun. Table 3 presents the experimental equipment specifications. Equipment and calibration details are presented in Appendix A2.

Table 3 – Experimental equipment specifications

Instrument	**Height [m_{agl}]**	**Scan [s]**	**Average [min]**
Cup anemometer Thies First Class	15.6	1	1 and 10
Wind Vane Thies First Class	14.0	1	1 and 10
Ultrasonic Anemometer Young 81000	17.2	0.05	60
Power transducer OHIO PC5	6.0	1	1 and 10
2D Inclinometer HL 5^{o}	16.6	1	1 and 10
Hygrothermal sensor Thies	14.3	1	10
Barometer Thies	9.0	1	10

Table 3 shows that measurements of wind speed and direction, as well as power output are collected at 1Hz and recorded at 1 min and 10 min averages, following IEC 61400-12-1 (Annex H). Sonic wind speed and temperature are measured at 20 Hz, following the flux measurement procedures already discussed. Temperature, humidity and pressure are

used to calculate the 10 min air density average. Appendix A5 shows a picture with each instrument height.

The CR1000 data logger is used for data collection. The script for data logger configuration, in CRBasic language, was developed to create different scan loops and data tables. As in Table 3, the 1 Hz scan covers all the variables apart from the sonic anemometer and creates a 10 min data table (AERO_10min) along with a raw 1 s data table for some variables (INCLI_1s). The 20 Hz scan records the sonic measurements, creating 60 min average flux measurements and a raw 20 Hz data table (AERO_20Hz). Each datable has a metadata specified in Appendix A3, which describes all recorded variables.

With 20 Hz flux measurements, the NL115 module is installed with a 2GB memory card in order to store the large volume of acquired data. Therefore, an important specification is the Data table Fill Time of 138 days, which dictates the maximum period without data collection on site. The NL115 module also has a direct Ethernet connection with the university network, enabling remote access at any time and collection of the 10 min data table. A GSM/GPRS modem is installed for the sake of communication redundancy. For time accuracy, a GPS Garmin 16x synchronize the station's clock every one second (GMT-3). Loggernet software is used for real-time monitoring and data collection.

3.3 EXPERIMENT LAYOUT

As already stated in Section 2.1.4, the chosen SWT location in this experimental setup aims neither for maximum power production nor undisturbed regions. The primary objective is to capture wind data and power collection at high turbulence levels, in a wind profile region that can be considered as being within the ASL.

A 1.7m height difference is noticed between the hub height (Table 2) and the sonic anemometer (Table 3), which is within the IEC tolerance. Since both cup and sonic measurements are going to be considered, a simple log law height correction is applied. Figure 14 shows the experimental setup layout, with equipment positioning, main obstacles and a measured wind rose at $17m_{agl}$.

Figure 14 – Experiment layout and measured wind rose at 17m_{agl}

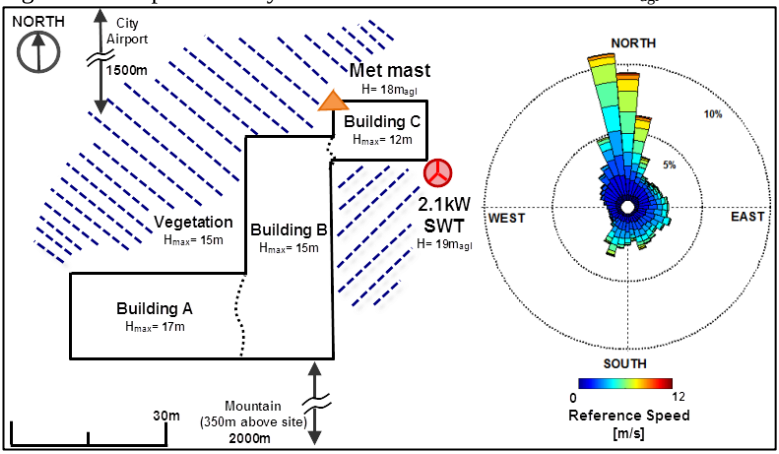

Equipment are installed in the northern building, with the met mast facing the prevailing northern winds, as shown in the wind rose (Fig. 14, right). Vegetation with trees and bushes surround the building area. Nevertheless, the experiment area is located in the University farm. Therefore, apart from the nearby obstacles the average roughness length is relatively small, since it is a non-urban area. Appendix A4 shows a 360^o view from the equipment.

The city airport is located around 1.5km away to the north and mountains, 350m high, are located 2km south. With a complex terrain nearby, high levels of ambient turbulence are expected, but at the same time flux measurements can be made owing to the surrounding open field. Table 4 summarizes the SWT and met mast positioning.

Table 4 – Equipment heights and locations

Small Wind Turbine	
Geographic Position:	27°41'1.40" S, 48°32'43.08" W
Altitude:	5 m
Hub height:	18.9 m_{agl}
Meteorological Mast	
Geographic Position:	27°41'1.00" S, 48°32'43.73" W
Altitude:	13 m
Height:	18.0 m_{agl}

As already discussed, this layout considers specific conditions of the urban wind profile, so that the ultrasonic anemometer is placed twice as high as the mean building height in order to capture the inertial sub-layer properties of the conventional ASL, where MOST can be applied.

3.4 DATA PROCESSING

With all data collected, a filtering procedure is necessary. As pointed in the logbook (Appendix A1), maintenance is necessary and also data logger failures occur. Thus, the first step of filtering is the time series consolidation. This method finds repeated data as well as gaps in order to construct a consistent database with continuous 10 min timestamps. A monthly consolidation process with quality flags aims to spot suspicious or unusable data. Figure 15 presents the 10 min flags.

Figure 15 – Data consolidation flags

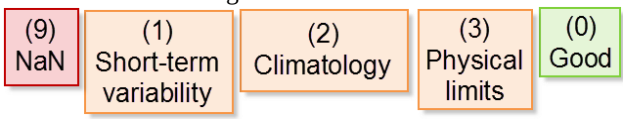

First, the continuous 10 min time series receives Not a Number (NaN) values with flag 9 in the analyzed variables: wind speed, wind direction, temperature, humidity and pressure. The short-term variability seeks to identify values that presented an unusual variation over 10 consecutive measurements (100 min), receiving flag 1 and being classified as suspicious. The flag 2 considers a climatology analysis, where suspicious data are classified when values are outside a $\pm 3\sigma$ control limit. Flag 3, called physical limits, labels as unusable data outside the sensor measurement range. If all tests are negative, that measurement receives the Flag 0 for good data.

Figure 16 shows the filtering result for wind speed measurements at 15.6m_{agl} with cup anemometer.

Figure 16 – Flag results for wind speed (cup anemometer)

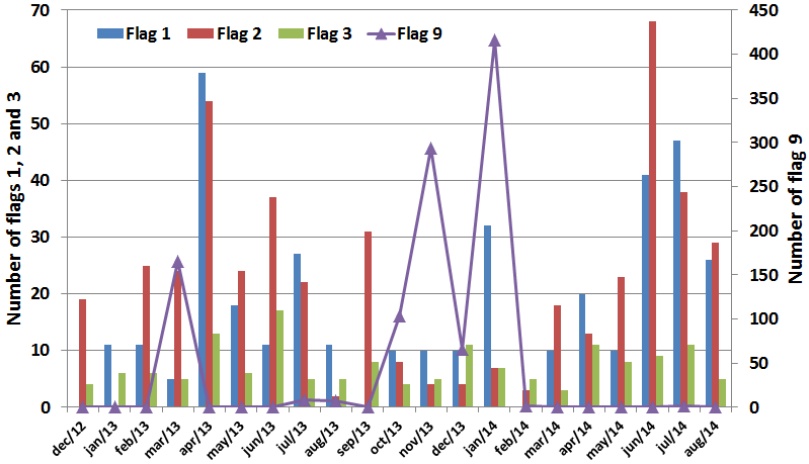

3.4.1 Flux Measurements

Before filtering, raw 20 Hz sonic data had to be divided into 20min individual files in order to handle the large amount of data. A shell script was developed for this division, and monthly time series were treated separately with EddyPro software.

The basic default configurations remained the same, but due to the high complexity terrain some adaptations were performed. A 10 min time series with the temperature, ambient pressure and temperature, called biomet data, performs flux corrections based on meteorological conditions.

For the advanced settings, sensitivity analysis was performed with different setup combinations, in order to evaluate the impact of each filtering and correction technique employed. EddyPro averaged data at 60-min intervals using linear detrending. Block average and the other methods clearly showed abnormal results.

With a large associated roughness length, the vertical velocity fluctuation (w') tends to be overestimated due to the influence of the building, resulting in incoming winds with a high angle of attack. Therefore, statistical filtering for spike removal and angle of attack aimed to minimize this effect.

A comparison between different rotation methods aimed to verify which calculation was best fitted for the studied site. Double rotation accounted for more realistic u_* values, where planar fitting was still presenting unrealistic values of w'. Although planar fitting is used for

urban canopies, a zero fluctuation plane, where $\overline{w'} = 0$, can not always match the actual flow distortion and show unreal results. Therefore, a double rotation in the most affected directions proved to be a better approach.

Another experimental tool was possibility of a real-time tilt analysis with the 2D inclinometer, since one-degree tilt can give 10% deviation in flux measurements (AUBINET; VESALA; PAPALE, 2012). Results showed less than 1^{o} tilt variation of the tower boom, evidencing that the larger errors come actually from flow distortions. Therefore, inclinometer data was only applied for a periodic met mast alignment with the ground.

Rainy days were identified based on airport data and were not analyzed in order to avoid dropout events, due to ultrasonic sensor obstruction. Even with this filter, the software performed drop-out tests as well as all the other available statistical filters.

EddyPro applied the steady-state filter as described by Vickers and Mahrt (1997). Hence, non-stationary conditions could be identified in alongwind and crosswind components, in order to filter conditions that would violate the MOST quasistationary hypothesis. The steady-state filter was actually one of the most important in the analysis, with the higher amount of data removal; even more than the angle of attack, as presented further. Table 5 summarizes the chosen configuration setup for flux measurements calculation in EddyPro.

Table 5 – EddyPro selected configuration setup

Configuration	Setup
Canopy height	5m
Measurement height	$17.2m_{agl}$
Detrend method	Linear detrending
Tilt correction	Double rotation
	Spike removal
	Drop-outs
Statistical Analysis	Absolute limits
	Angle of attack
	Steadiness of wind

The output data is presented in a comma-separated file, including all the necessary parameters to evaluate atmospheric stability based on Obukhov length, as well as raw flux measurements, meteorological variables and the flags for each selected filter. The full output metadata is described in the software manual (LI-COR, 2013).

Lange and Focken (2006) consider the absence of a sonic anemometer for Obukhov length calculation, measuring velocity and temperature at different heights and evaluating their gradient. Arya (2001) presents this approach as the bulk transfer method, which can be understood as a half-order closure, because it parameterizes the flux measurement (STULL, 1988). With this approach, friction velocity can be estimated by a bulk drag relation (Eq. 4.1).

$$\tau = \rho u_*^2 = \rho C_D U^2 \quad \therefore \quad u_* = \sqrt{C_D}\mathrm{U} \tag{4.1}$$

Where C_D is a drag transfer coefficient. In order to verify possible deviations in friction velocity values calculated with eddy covariance, mainly due to building influence, the bulk transfer method will be used as a validation threshold.

Garrat (1977) presents a study evaluating drag coefficient values at distinct areas. A value of $C_D = 0.026$, applied for forest canopies in South America, will be used in the correlation between eddy covariance and bulk transfer methods. This correlation of distinct flux calculation methods was borrowed from large wind turbine studies (PEÑA; HAHMANN, 2012).

3.4.2 Stability Classification

Wharton and Lundquist (2010) performed a power performance study with large wind turbines as a function of TKE, TI, wind shear and L, with a proposal for atmospheric stability classification based on all the this parameters. With a proper estimation of the Obukhov length, L, this work will adapt the classification of this.

Since the work isn't focused on wind profile correction and validation, the classification will consist of three main categories: unstable, neutral and stable atmospheres. This classification goal is to capture the daytime net upward heat flux and vice-versa, so that power collection deviations can also be categorized. Table 6 presents the adopted atmospheric stability classification.

Table 6 – Atmospheric stability classification

Stability	**Obukhov Length, L [m]**
Stable	$0 \leq L < 400$
Near-neutral	$L \geq 400$ or $L \leq -300$
Unstable	$-300 \leq L < 0$

4 RESULTS AND DISCUSSION

The first important result is the operational experimental setup constructed for this case study that, after some pitfalls, only needs the scheduled maintenance to operate properly from now. Secondly, it is worth mentioning the size and importance of the dataset collected so far, with power output, wind regime and flux measurements summing 15,217 hours of valid data, from November/2012 to August/2014, which results in a recovery rate of 98.84%.

LEPTEN laboratory will continue the data collection, increasing the database that will undoubtedly be used for further studies. The following results and discussion are based on these two main accomplishments.

4.1 WIND REGIME

As already discussed, the first step for wind resource characterization is a statistical description of the local horizontal wind speed with the Weibull distribution (HENNESSEY, 1977). Since the database has two wind speeds, from cup and sonic anemometers, an inter-comparison can be made. Figure 17 presents Weibull distributions for both cup and sonic measurements. All the results from this section comprehend the period from November/2012 to August/2014, except for the sonic anemometer, that started operation in March/2013 (Appendix A1).

Figure 17 – Weibull distributions for cup (a) and sonic (b) anemometers

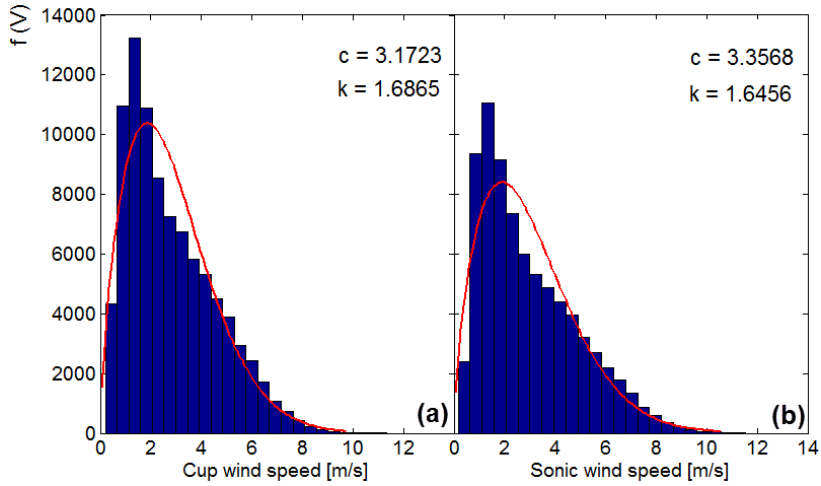

There is a variation in shape (k) and scale (c) Weibull parameters between the two distributions, but they are considered acceptable due to the height difference of 1.6m. One observed fact is that wind distribution in complex terrains does not necessarily have a Weibull-like behavior.

Likewise, measured wind roses from the wind vane and sonic anemometer (Fig. 18) also show different regimes. Hence, wind speed and direction are affected by building and vegetation influence, although with little impact in 10 min average regime, with both wind sensors presenting a consistent wind characteristic.

Figure 18 – Wind roses from wind vane (a) and sonic anemometer (b)

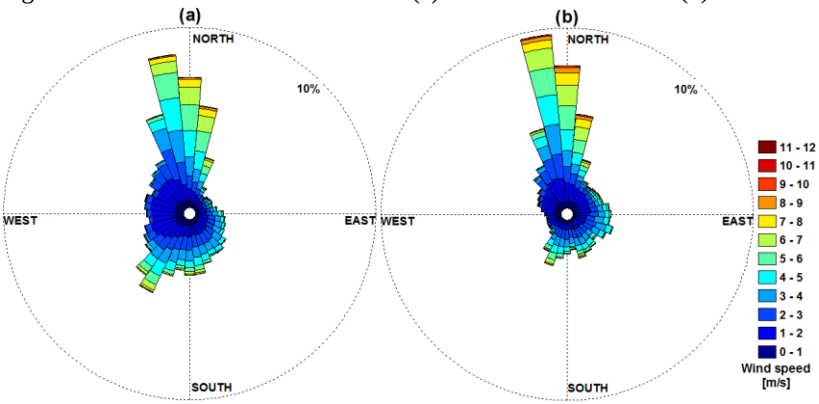

Sonic measurements tend to be more representative as they are placed at hub height of the SWT. However, the high roughness effect requires a validation between the sonic and the certified cup anemometer and wind vane. With that in mind, the wind rose is divided into 16 sectors. Figure 19 shows the 22.5^{o} sectors matching the cardinal and ordinal directions.

Figure 19 – Sector analysis division

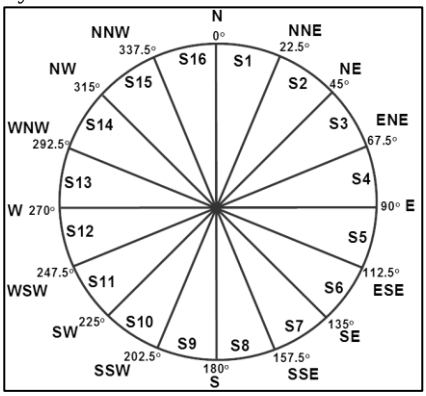

Comparing the sector division (Fig. 19) with the experimental layout (Fig. 14), it's possible that each sector can give a different contribution for the observed deviations. However, based on the wind roses presented on Fig. 18, two main regions are going to be chosen for a sector analysis, in order to simplify the study: a northern sector, from NNW to NNE, and the southern sector, from SSE to SSW. This sector unit is also going to be used in the power curve analysis in Section 4.4.1.

Figure 20 shows the correlations among the two wind speed and wind direction sensors. A fair wind speed correlation is observed, with a correlation coefficient $R^2 = 0.961$ for all sectors, but with two strong tendencies well divided. With the sector analysis, these deviations are evidenced as being sectorial trends, as presented in Fig. 20a.

Figure 20 – Wind speed (a) and wind direction (b) correlation

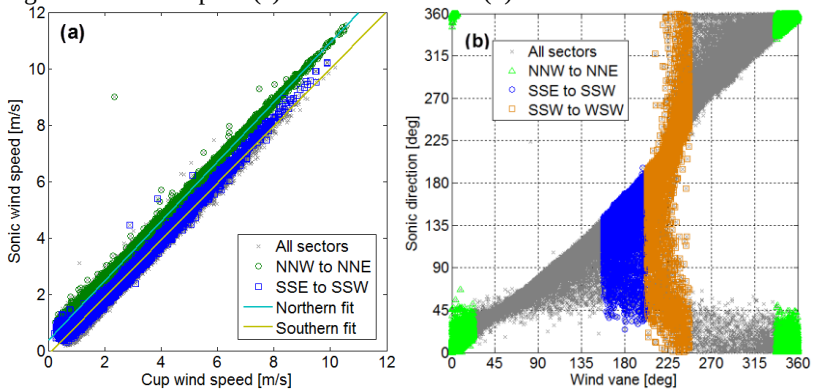

For the northern sectors (NNW to NNE), the wind speed presented a perfect correlation, $R^2 = 0.998$, with an offset of $+0.38 m/s$, due to the

height difference. Additionally, the southern sectors (SSE to SSW) also showed a lower correlation, $R^2 = 0.990$, with a $-0.11 m/s$ offset, indicating a higher obstacle imprint. Therefore, the sonic wind speed is validated and sector analysis demonstrates a lower building influence of winds coming from the northern sectors.

However, concerning the wind direction (Fig. 20b), the sector analysis shows a great dispersion in the sonic direction values. Since the sonic anemometer composes a wind vector based on the measured wind components, small deviations caused by flow recirculation or streamline discrepancy can drastically alter the resultant wind vector angle.

Because of high turbulence levels, significant deviations are observed in the wind direction mainly from the southern (SSE to SSW) and west-southern sectors (SSW to WSW). The northern sector, already considered with low building influence, presented a fair correlation. Hence, wind vane direction values are going to be considered in further analysis.

Following the same sector analysis procedure, the wind diurnal cycle is presented in figure 21 as a function of the wind sectors. This surface, called daily wind regime surface, shows in a straightforward way the variation of the wind speed during the day as a function of the wind sectors. The surface is composed by the sonic wind speed with wind vane direction.

Figure 21 – Daily wind regime surface

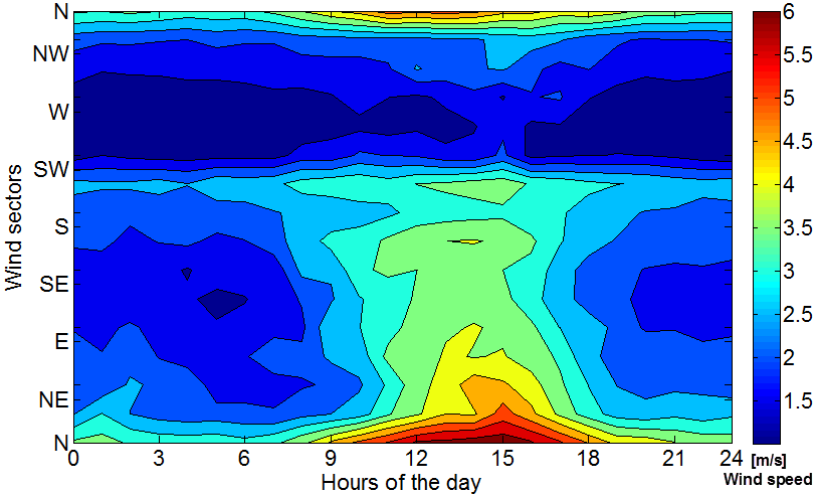

The wind regime confirms the occurrence of relatively low wind speeds, as expected. The daily peak is on average 3 m/s higher than the

SWT cut-in wind speed, around 15h. The surface also agrees with the wind rose, but adds further information, with higher wind speeds from the E and SE sectors at peak time.

This phenomenon was observed during SWT monitoring and reported in the logbook (Appendix A1), as high turbulent winds without a well-defined direction. During days with this regime the SWT wouldn't start, even with wind speeds higher than 4 m/s, since it could not reach a proper alignment.

It seems from this observation that southern winds tend to be less constant, therefore with higher standard deviations. Turbulence intensity (TI) is thus analyzed. Figure 22 presents the TI distribution as a function of the wind speed. The sector analysis was also applied. With the application of the IEC bin method, binned TI curves for the different sectors could be calculated. Values of TI for wind speeds lower than 2 m/s are considered to be unrealistic.

Figure 22 – Turbulence intensity analysis

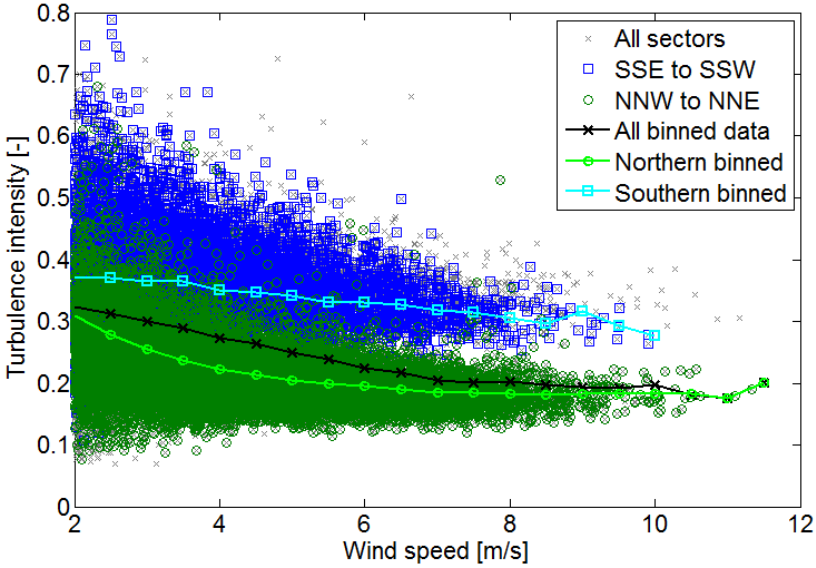

The southern sectors show higher TI values for the entire wind speed range, confirming to be more affected by the nearby obstacles. During the collection period the average TI was 31.5%, with a standard deviation of 13%. The northern sectors presented a TI of 24.1% ($\sigma = 0.1$) and the southern sectors a TI of 37.2% ($\sigma = 0.11$). Therefore, northern winds are more frequent, as pointed in the wind rose, as well as

more regular. The sector analysis proved to be an effective tool for wind regime characterization in complex terrain.

Since there is more than one year of collected data, it's possible to perform an annual analysis, such as seasonal effects and cumulative distributions over the year. Appendix B presents a table with monthly averages for the main variables. Monthly data evidence significant site-specific aspects, like local air density, which need to be considered in power curve calculations.

Figure 23 shows a map for the annual wind speed regime. The site seasonal effects become evident, showing higher values for wind speed during summer time, with peaks between November and February. The daily wind regime is maintained throughout the year, with higher values between 12h and 15h.

Figure 23 – Annual wind regime surface

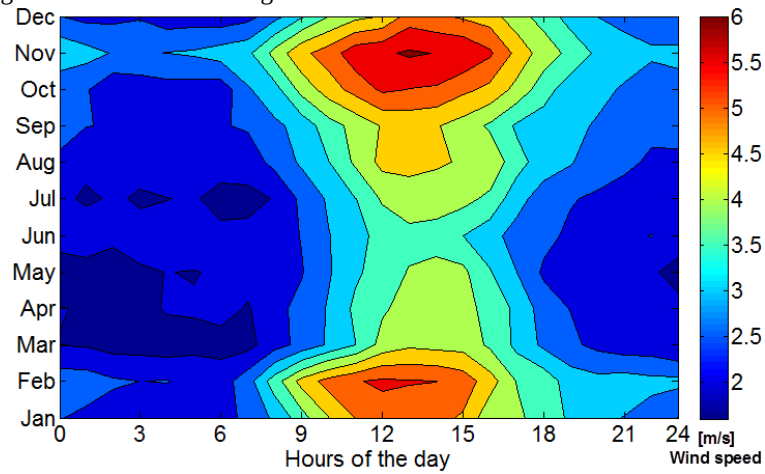

A common analysis for annual wind data is the cumulative wind distribution over time. The standard year has 8760h; hence,

Figure 24 presents the local wind distribution over a typical year. As expected, a low wind regime is observed, with wind speeds higher than 6 m/s being measured at 10% of the time.

Figure 24 – Wind speed cumulative distribution

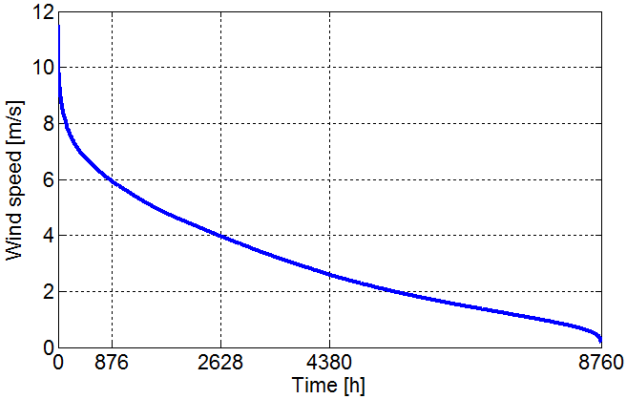

A similar distribution might be expected for power output. Rated power output cannot be observed, and the SWT can have an efficient power production during only 1/3 of the year (above 4 m/s). Energy production results are presented in Section 4.3.

4.2 DATASET

Power performance analysis and flux calculations are performed with a limited dataset. The six month period from December/2013 to May/2014 was selected.

Different filters were used in order to obtain usable data both for power curve construction as well as for atmospheric stability assessment. Table 7 presents a summary of the used dataset with the applied filters. Two basic divisions were adopted:

- Dataset I, IEC-based: Filter for regular SWT operation data, that is going to be used for power curve construction;
- Dataset II, Stability-dependent: Filters for valid turbulent flux measurements, in order to classify stability conditions.

Table 7 – Dataset division with applied filters

Dataset	Filter Procedure	Data (hours)	Recovery Rate
IEC-based (I)	(a) Raw data	4287	98.2%
	(b) Power output	3932	90.0%
Stability-dependent (II)	(c) Rain Threshold	3919	89.7%
	(d) EddyPro QC	3428	78.5%
	(e) Steady flow	1133	25.9%

Dataset I start from the raw data and removes data of SWT's non-operational occurrences for the analyzed period, resulting in a 93.3%

recovery rate. This amount of data, with 4074h, is already sufficient for the power curve determination and the IEC 61400-2 duration test. The stability-dependent Dataset II aims to include further filters in the flux measurements processed by EddyPro.

Filter (c) removes rainy days, in order to avoid drop-out events and to consider days with high sensible heat flux values during daytime. Some statistical filters in EddyPro software, such as angle of attack, only add flags to the metadata, without correcting the values. Therefore, filter (d) removed hard-flagged data, with an angle of attack value higher than 30^{o}.

The quasi-stationary filter is also represented with flags in EddyPro. Along with the angle of attack, this was an important criterion in the flux measurement analysis, since the local conditions are highly turbulent and with high variability, both in wind speed and direction. The steady flow criteria, given by Vickers and Mahrt (1997), removed more than 1000 hours of data, leaving Dataset II with 29.3% of recovery rate. This final dataset is used in the stability-dependent power curves shown in Section 4.5.

Table 8 presents some environmental conditions within Dataset I, which are usually reported in power performance tests. The studied site has a subtropical climate, without extreme temperatures, without events such as icing or overheating. From the instantaneous (1 Hz) power value, it can be said that the used power transducer (up to 5kW range) was well-specified. As for the 10 min data, the SWT did not reach the rated condition during the analyzed period.

Table 8 – Environmental conditions during test period

Description	Value
Highest instantaneous wind speed	20.5 m/s
Highest instantaneous power	4792 W
Highest 10min wind speed	10.8 m/s
Highest 10min power	2074 W
Highest 10min temperature	35.5 ^{o}C
Lowest 10min temperature	10.6 ^{o}C
Turbulence intensity @ 11 m/s	17.5 %

As already discussed with the TI distribution, this site is considered to have a complex terrain and high ambient turbulence levels. IEC recommends the specification of TI at 15 m/s, but as a low wind regime was observed this range could not be achieved.

Another IEC requirement concerns the range of valid wind speed bins given in the measured power curves. Filled bins should cover a

range from 2 m/s until 14 m/s in the given case. However, as presented in table 7, this requirement was not met.

Therefore, apart from higher wind speed bins (>12 m/s), collected data was sufficient to meet IEC requirements for power performance assessment (IEC, 2005, 2013). The raw dataset, as well as the used CRBasic script, are available upon request.

4.3 SWT OPERATION

Figure 25 shows a three days period, that represent the regular SWT operation, with power output, wind speed and wind direction data. Winds from the northern sectors in the first two days show a constant energy production during daytime, with lower values during the night, as expected by the diurnal cycle. In the third day, winds come from southern sectors with lower intensity, when the SWT cease the generation.

Figure 25 – SWT regular operation regime

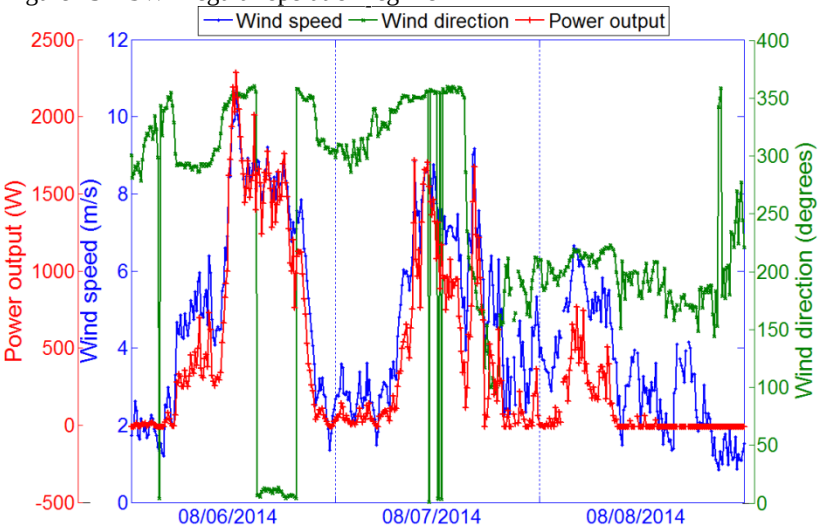

Skystream 3.7 is a downwind turbine, or else the blades are in a downwind position of the nacelle, therefore not facing into the wind as is the case of turbines with yaw drive control. One of the issues of this configuration is the necessity of a minimum amount of drag, so that the turbine can align itself with the prevailing wind and start operating.

As spotted in the daily wind regime plot (Fig. 21) and reported in the logbook (Appendix A1), during winds from E and SE sectors the

turbine cannot achieve a proper alignment. Figure 26 shows this failure of the passive yaw control under an unsteady wind regime.

Figure 26 – Nacelle misalignment with prevailing wind

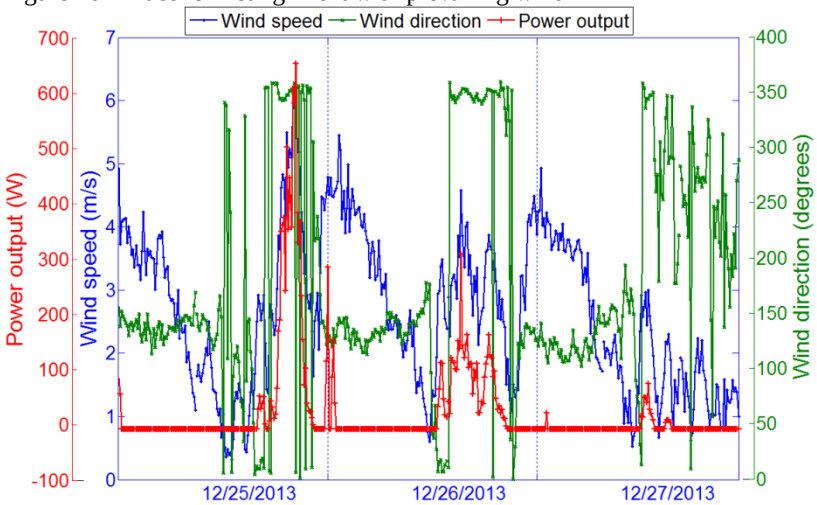

For the three consecutive days presented in Fig. 26 a similar wind regime is observed. With wind speeds above the cut-in the SWT does not generate power, particularly when wind is coming from the east and southeast. This type of wind regime is commonly known in the region for its gusty behavior along with fast changes in direction.

During the six month period of analysis, from December/2013 to May/2014, the SWT presented a reliable operation, as defined by IEC 61400-2, with no significant failures, no corrosion or damage to the turbine components and an operational fraction time (OFT) of at least 90%.

Because of the SWT relocation, there was excluded data due to shut down in the first 10 days of December/2013, with $T_T = 4287$, $T_N = 200$ and $T_E = 232$. Therefore, the OFT (Eq. 2.10) can be calculated as,

$$OFT = \frac{4287 - 200 - 232}{4287 - 232}(100\%) = 95.1\% \qquad (4.1)$$

It is worth noting that OFT cannot be considered the same as the recovery rate, since excluded data does not count as valid. With a reliable operation, Table 9 presents further requirements for the duration test.

Table 9 – Hours of power production during test period

SWT Class II – V_{ave} = 8.5 m/s			
Wind speed	Measured [h]	Required [h]	Pass/Fail
>0 m/s	3932	2500	PASS
>10.2	0.2	250	FAIL
>15.3	0	25	FAIL
Operation	Measured [%]	Required [%]	Pass/Fail
Fraction Time	95.1	90.0	PASS

With the low wind speed regime, the studied SWT only passed in the first minimum required service time of 2500h at any wind speed. Since higher wind regimes were not observed during the full measurement period, the SWT will probably have a reliable operation throughout its lifetime.

Concerning power output, Figure 27 shows the monthly energy production (MEP) for the selected test period. It also presents the respective Capacity Factor (CF), which can be understand as an efficiency parameter, given by the total production in that period divided by the maximum possible production (rated power x time). The cumulated electricity generation for the test period is 429.6 kWh, which corresponds on average of a CF equals 5.0%.

As discussed by Wood (2011), small wind applications in urban environments tend to underutilize the SWT capacity. In terms of contribution to the building electricity consumption, it cannot be said that the equipment had a significant impact nor that the application is economically viable, as already stated by Santos (2011) and Santos et al. (2011).

Figure 27 – MEP and CF for the analyzed period

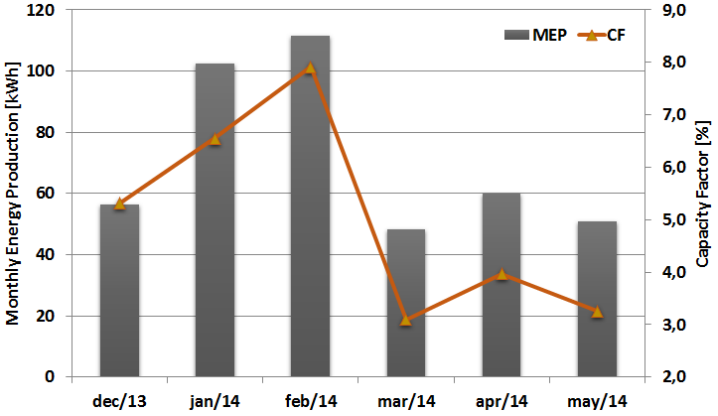

According to IEC 61400-12-1, wind turbines performance assessment is based on the power output database, collected continuously at a sampling rate of 1 Hz. Mean power output with maximum and minimum values, as well as the standard deviation, should be recorded in 10-min intervals. Figure 28 shows the 10-min collected dataset.

Figure 28 – 10-min power performance dataset

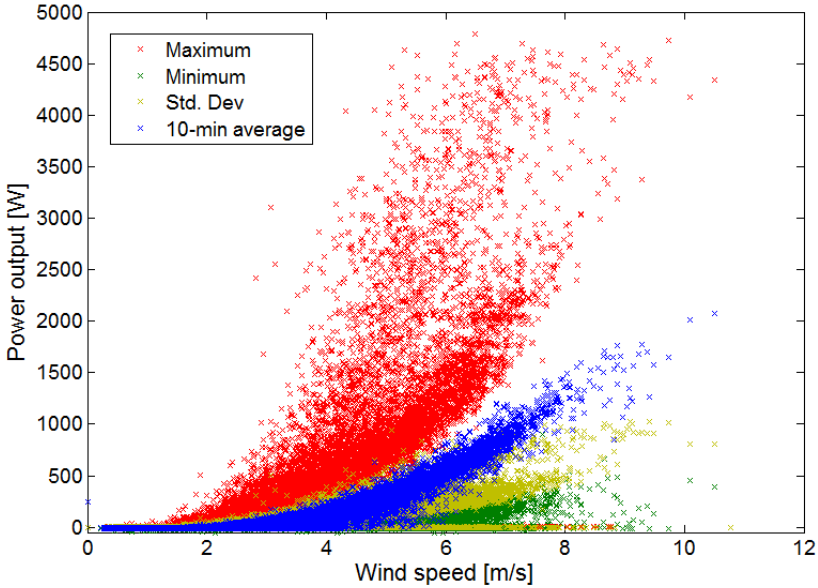

This 10-min based dataset is used to construct a power curve comparable to the Skystream 3.7 certification (WINDTEST, 2009), which also presents data in 10-min averages. However, for small wind turbine assessment, IEC gives a particular set of recommendations in Annex H (IEC, 2005).

For small wind turbines, along with the 1 Hz sampling rate, dataset shall be of 1-min duration. Therefore, all 10-min averages, corrections and calculations shall apply to this dataset. The possible main reason for this shorter averaging period is to better capture the SWT behavior in unsteady, or turbulent, conditions.

Figure 29 presents the 1-min dataset for the analyzed period. This dataset is the base for power curve measurements, as well as stability-dependent and TI-dependent analysis, presented in Section 4.5.

Figure 29 – 1-min power performance dataset

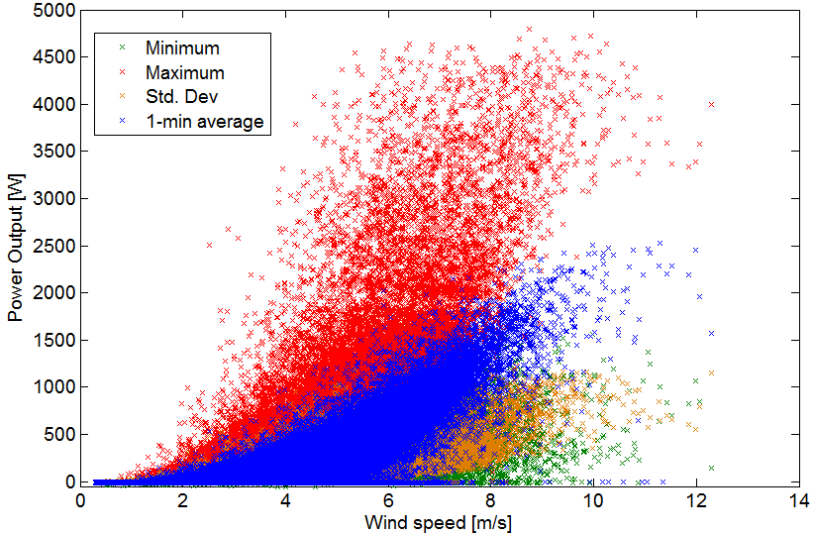

4.4 POWER CURVES

With filtered 10-min and 1-min datasets, it is possible to trace the measured power curves for this case study. The so called IEC-based power curve was first traced for the 10-min dataset, with the objective to compare the SWT power performance with the certified, and therefore expected, manufacturer curve.

Appendix B presents the average site's air density of 1.191 kg/m^3 ($\sigma = 0.018 kg.m^{-3}$), which is lower than the IEC standard of 1.225 kg/m^3 and, therefore, needs to be normalized. Equations 2.2 and 2.3 were used, with velocity and power output data corrected to the reference density. Standard uncertainty bars, Eq. 2.4, are plotted as possible error intervals. The IEC bin method requires that, for a 10-min dataset, all the plotted bins must be filled with, at least, 30 min of valid data, thus with a minimum of three experimental points per bin. Figure 30 presents the 10-min power curve plotted with IEC requirements along with the certified curve. The power coefficient curve is also plotted with the same corrected binned data.

Figure 30 –IEC 10-min power curve vs. manufacturer

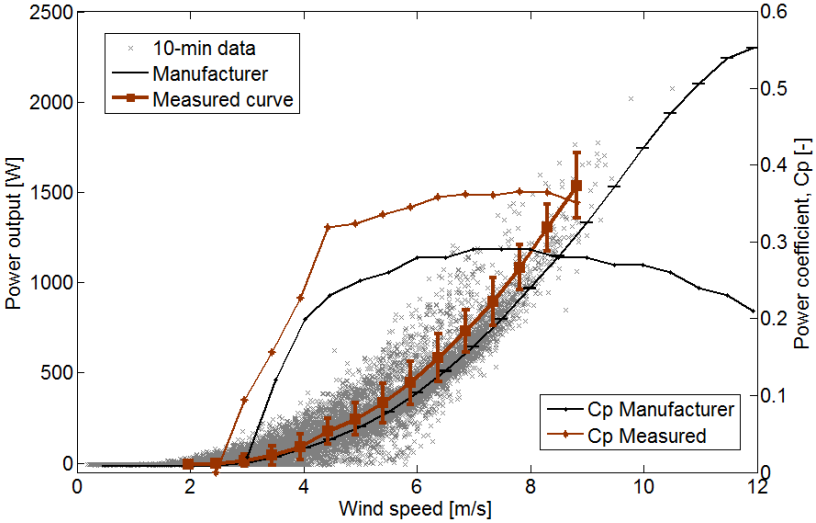

A performance above the expected, with an average power output 13.6% higher than the manufacturer data is observed. However, only low wind speed bins were filled, without capturing the behavior at close to the rated condition. This behavior can be understood considering the high values for local turbulence intensity, with an average TI of 32%, in comparison with 9% on the site of the certified curve.

With higher speed standard deviations, “negative fluctuations” are limited by the cut-in condition at lower wind speeds, where only “positive fluctuations” will be converted to power, therefore increasing power collection for higher TI levels at the ankle power curve region. Previous results from other studies with TI also show the same behavior, both in experimental measured data (LUBITZ, 2014) as with numerical simulations (SUNDERLAND et al., 2013).

The 10 min scattered experimental data also indicates the influence of nearby obstacles, as already shown in the sonic anemometer correlation in figure 20, with two main trends: one that follows the manufacturer curve and some points with higher energy collection. Thus, a sector analysis will also be presented for the power curves, in order to spot the observed deviations.

Following the power performance special requirements for SWT, the IEC-based 1 min power curve was also traced. With a smaller averaging period, flow instabilities at higher frequencies are better captured. Hence, we can assume that smaller turbulent scales are better

represented in the 1 min power curve, when compared with the 10-min manufacturer curve (Fig. 31). In this case, bins are considered filled with 10 min of data (IEC, 2005), that is a minimum of 10 experimental points. The manufacturer power curve is also plotted, but no direct power collection comparison can be made with distinct average intervals.

Figure 31 – IEC 1-min power curve vs. manufacturer

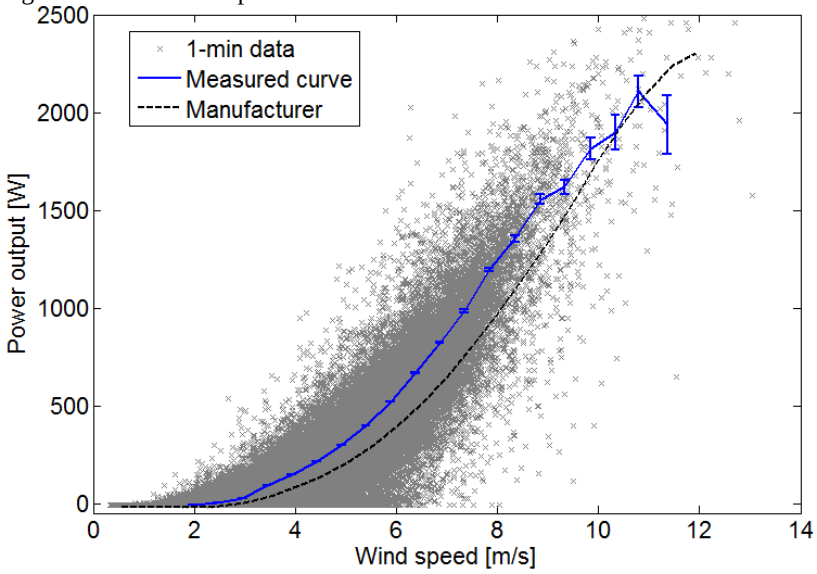

The 1 min measured presents a decreasing power collection behavior that starts at 8 m/s, considered premature when compared with the expected curve, where the knee region is closer to the rated wind speed of 11 m/s.

Wood (2011) points out the role of control strategy, especially in the region close to the rated condition, where the SWT is not able to respond in an optimal way to the fast and large fluctuations of wind speed. Local stall situations can occur on the rotor blades, thus resulting in underperformance.

Therefore, probably at above 8 m/s the “positive” fluctuations” are limited by the SWT’s power control system, where only “negative fluctuations” will be converted to power output. In order to evidence flow pattern effects, stability-dependent power curves aim to assess power collection deviations caused by turbulent transport of heat and momentum along the ASL.

4.5 STABILITY-DEPENDENT PERFORMANCE

After processing, friction velocity (u_*) results could still have building influence. In order to remove this effect, a correlation between two distinct flux calculation methods is applied. The sector division already presented in Section 4.1 is used to evaluate deviations in friction velocity estimation, with a comparison between eddy covariance and bulk methods.

From figure 32, it is clear that sectors from NNW to NNE had higher u_* values. Therefore, wind directions from 337.5° to 22.5° can be considered in disturbed sectors for this parameter. For the Obukhov length calculation, values from this sector were corrected with a linear correlation with the bulk friction velocity.

Figure 32 – Friction velocity correction for disturbed sector

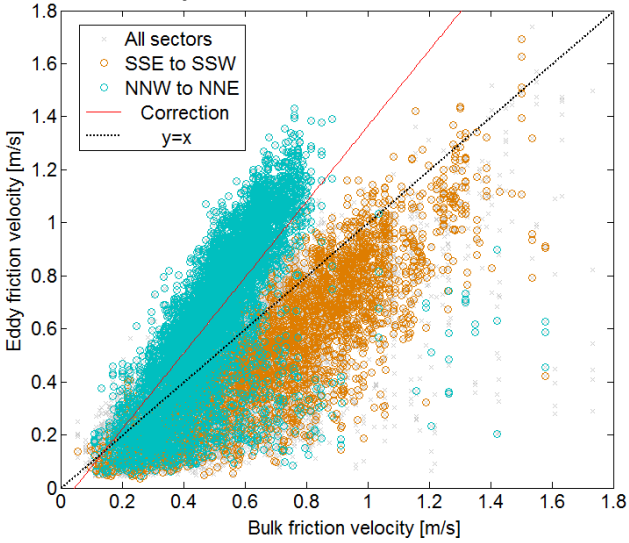

Figure 33 presents the results for Obukhov length calculation and division into stability classes of Table 6. A histogram of L in figure 33a shows the proportion of each condition in the studied site.

Unstable conditions are predominant with 53% of occurrence, and stable conditions account for 42% of the time. Near-neutral atmosphere is usually characterized under higher wind speeds, where neither mechanical nor thermal turbulence generation is relevant. Therefore, it isn't a surprise to observe only 5% of this condition on site.

Figure 33 – Obukhov length histogram (a); stability diurnal regime (b).

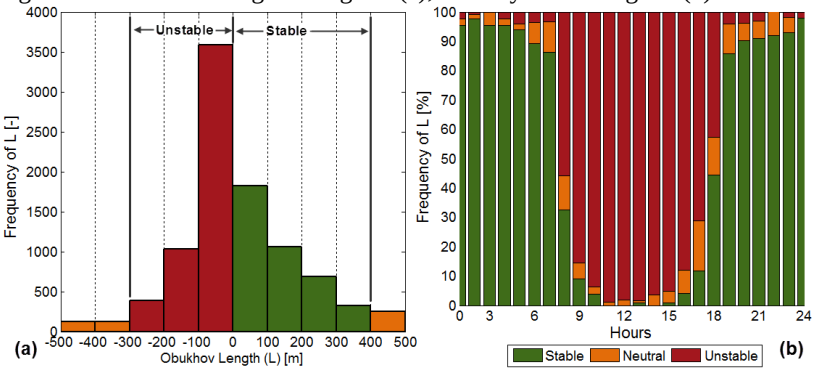

Figure 33b shows the daily regime of L. As expected through the previous discussion, unstable conditions, with higher vertical transport of momentum and heat, are observed during the day. At night, with a downward net heat flux, the thermal component consumes the mechanical shear, hence reducing turbulence levels.

The IEC 1-min power curve is now segregated into the atmospheric stability classes presented above. The overall measured curve is taken as a reference, and stability-dependent curves are constructed based on Obukhov length. Since the turbulence intensity was used so far by SWT performance assessment studies (LUBITZ, 2014; SUNDERLAND et al., 2013), this parameter is also used herein to compare both methods of ambient turbulence analysis.

Therefore, the threshold of $TI = 0.17$ will divide high and low turbulence conditions, defining the TI-dependent power curves. Figure 34 presents the stability-dependent and TI-dependent power curves for the analyzed period.

Figure 34 – Stability-dependent and TI-dependent

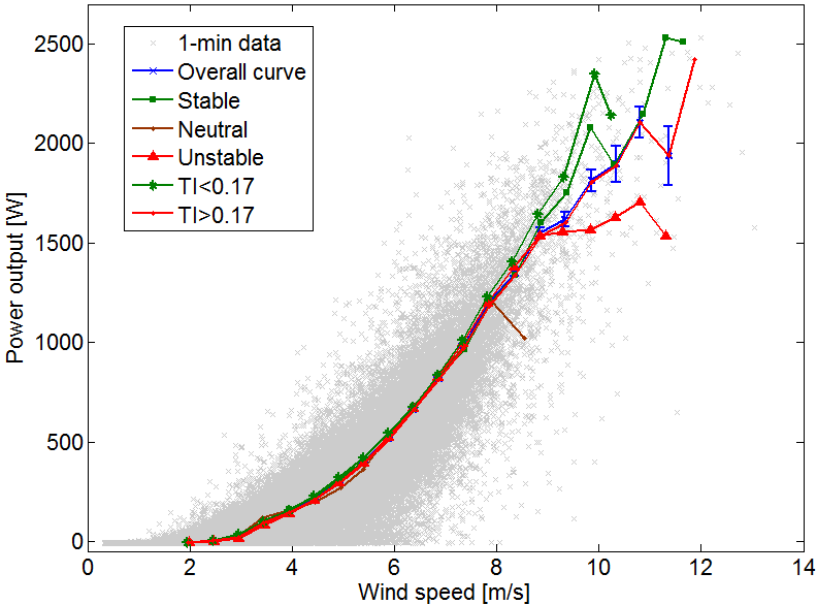

It is noticed a similar behavior of all curves on the ankle region. No major deviation from the overall was observed up to 8 m/s, neither for the TI-dependent curves, as in the work of Lubitz (2014), nor for the stability-dependent curves.

Above 8 m/s, nonetheless, atmospheric stability classification starts to evidence the decreasing tendency in power collection. With an effective mixing as well as both mechanical and thermal turbulence, unstable conditions present a lower power collection at the knee region.

In the other hand, the TI parameter could not spot the declining trend in power collection. High TI conditions can be correlated with unstable data, due to this convective mixing of momentum. However, for high TI data above 8 m/s, no major variation was observed.

At higher wind speeds, a same value of standard deviation has a smaller impact over larger wind speed averages; hence small TI values are predominant. The statistical limitations of TI parameter can be overcome with the use of Obukhov length as a physical measure of turbulent mixing inside the ASL. Therefore, this work proposes an approach for SWT power performance that encloses both TI and Obukhov length as classification criteria.

4.5.1 Stability and TI combined approach

Elliot and Cadogan (1990) related power output with TI, as presented in equation 2.9. This relation can be applied to the 1-min data, in order to give an estimate of the power curve for a fixed TI level. The average site TI was used to trace a TI estimation curve. Figure 35 presents a comparison between the IEC 1-min curve and the proposed TI estimation.

Figure 35 – IEC 1-min power curve vs. TI estimation curve

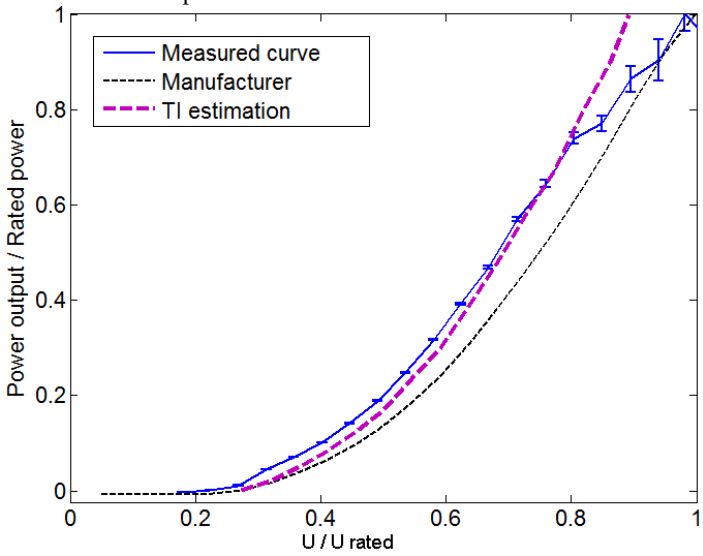

The presented power curve is normalized with the rated condition. The TI estimation tends to increase the power collection at lower wind speeds, getting closer to the actual measured power. However, from 8 m/s onwards this estimation does not account the non-linear power curve behavior, missing the measured premature knee region after the curve's inflection point, where $\frac{\partial^2 P}{\partial U^2} < 0$.

Consequently, TI parameter can be appropriate to represent and explain the SWT behavior in high turbulence environment, as urban zones, for lower wind speeds in the ankle power curve region, where $\frac{\partial^2 P}{\partial U^2} > 0$. Close to the rated condition, however, atmospheric stability needs to be included to account for the decreasing power tendency. Therefore, the presented results indicate that a new kind of analysis must be made for close to rated conditions, due to TI's statistical nature.

Figure 36a presents the stability and TI-dependent curves for the knee region, above 8 m/s. To better illustrate the measured variations for each classification, figure 36b shows the average power collection deviations from the IEC 1-min overall power curve.

Figure 36 – Specific power curves (a); Deviations from overall (b).

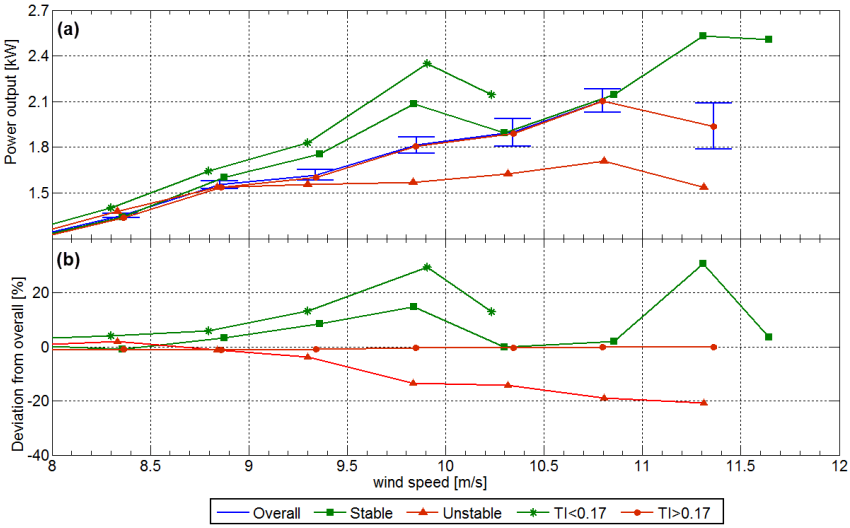

It´s clear that turbulence intensity (TI) parameter could not capture the overall power decreasing pattern above 8 m/s. Higher TI levels ($TI > 17\%$), that should represent the unstable condition, were not properly captured, since high wind speed bins tend toward lower standard deviations. In contrast, for the stability-dependent analysis, an average increase of 4.9% in power production was measured under stable conditions, while unstable conditions led to a production 4.6% below the average. Deviations up to 51% were observed between stable and convective conditions.

Close to the rated wind speed, the atmospheric stability parameter was able to provide evidence towards the observed tendency of a decrease in energy collection. Lubitz (2014) presented a similar study only with TI parameter, and did not encounter consistent results above 8 m/s. Hence, the proposed hybrid approach, combining TI and Obukhov length, can be a more precise way to assess the SWT power collection.

It is important to consider a larger quantity of data in the region above 8 m/s, in order to better confirm the presented average deviation values. IEC standard for filled bins were followed, but more data can surely increase the reliability of this results.

Since the instrumentation used for this study is not commonly employed in wind energy applications, one important issue is how to make atmospheric stability assessment feasible with the current sensors used in the industry. In large wind turbine applications, remote sensing instruments (SODAR and LiDAR wind profiles) are being increasingly used to assess wind farms performance (SATHE; GRYNING; PEÑA, 2011; WAGNER et al., 2011; WHARTON; LUNDQUIST, 2012).

Concerning SWT applications, further studies can be conducted with measurements for pollutant dispersion, urban thermal comfort and other usages that require fast-response sensors in the urban zone. Carpman (2010) used stability results in tall forest canopies to assess flux measurements in an urban zone. This study gave origin to some turbulence considerations in the safety requirements of IEC 61400-2.

4.5.2 Sector analysis

Wind measurements in a complex terrain showed to be highly dependent on wind direction. Likewise, a sector analysis for measured power curves should also lead to a better comprehension of the atmospheric stability distribution. Therefore, the normalized IEC 10 min power curve is divided into a northern sector, covering NW to NE directions (315^{o} to 45^{o}), and in a southern sector, from SE to SW directions (135^{o} to 225^{o}).

Figure 37 – Power curve sector analysis

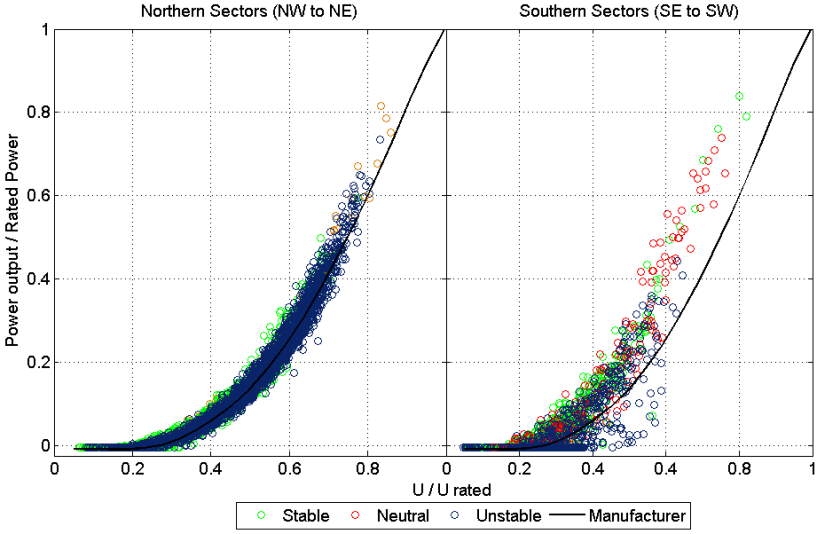

The power curve sector analysis shows that the average performance increase of 13.6% from the manufacturer curve can have a contribution from gusty winds, coming from the southern sectors and classified as atmospherically neutral. Analyzing the northern sectors, measured power curve fits the expected behavior from the manufacturer, where nearby obstacles have less influence in the power collection.

Terrain complexity presented itself as a major challenge for SWT power performance assessment. In the given case study, the experimental setup was focused on capturing the conditions of the incoming near-building flow, but was not necessarily designed for optimal flux measurement sensor location. Therefore, the aim of data filtering procedure was to minimize distortions and unrealistic values, caused by flow interaction with high roughness obstacles. Sector analysis was also a valuable tool. It should be noted that acquiring unbiased high-resolution wind and power output data from sensors and wind turbines in urban environments is an arduous task.

4.6 POWER SURFACES

IEC standard still lacks a procedure for SWT power performance assessment under high TI conditions. Sunderland et al. (2013) comments that IEC 61400-2 have turbulence considerations for safety, but nothing related on how to measure performance in high turbulence environments. The new edition of IEC 61400-12-1 is probably going to bring a power curve normalization for turbulence, as the Annex M (MELLINGHOFF, 2013). However, the results point out limitations for statistical turbulence parameters, hence normalizing power output with atmospheric stability can be introduced to account for the observed deviations.

It’s important to recognize the inherent limitations of normalization procedures, that still consider the power curve as a two-dimensional correlation between wind speed and power output. Likewise the given power output relation in equation 2.9 that includes the TI parameter, the presented results show the SWT power output dependence on atmospheric stability. Since wind energy collection is, therefore, multi-variable, this work introduces a concept which is also not included in IEC power assessment tools, with a multi-variable power curve, called herein power surfaces.

Figures 38 and 39 present two 3D power surfaces for both parameters analyzed in the present work, Obukhov length and turbulence intensity.

Figure 38 – 10-min stability power 3D surface

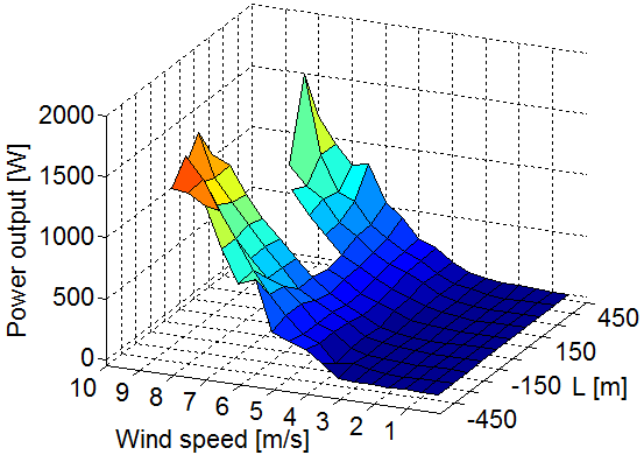

In the power 3D surface, it is possible to notice two distinct regions: an ankle region, at lower wind speeds, that are not influenced by the third parameter (TI or L) and a knee region, where turbulence starts to impact the power collection. The stability-dependent surface (Fig. 38) shows different behavior in stable and unstable conditions, with high values for stable and neutral conditions, as expected. Likewise, the TI-dependent surface (Fig. 39) evidence a higher power collection for lower turbulence events, characterized as stable conditions in Fig. 38.

Figure 39 – 1-min TI power 3D surface

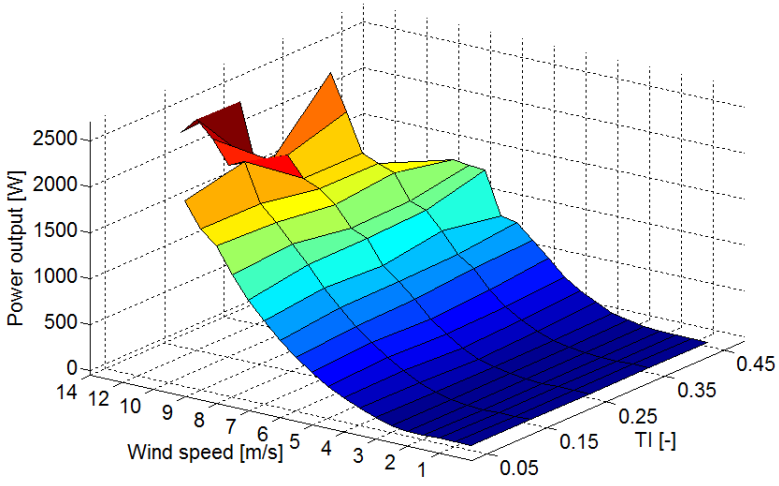

In order to better distinguish the power surface regions, figures 40 and 41 present a 2D surface, with the power output as a color bar. With the 2D surface is possible to evaluate the actual variation of energy collection along a specific wind speed or turbulence parameter.

Figure 40 shows the variation of power collection with Obukhov length. The white rectangle indicates an undisturbed area, where the turbulence parameter has almost no effect on power output. Therefore, within this region the idea for a power curve is still valid. Outside the rectangle, for higher wind speeds, the plot starts to justify itself. For 8 m/s, for example, the higher power collection for stable conditions is noticeable when compared to the unstable region.

Figure 40 – 10-min stability power 2D surface

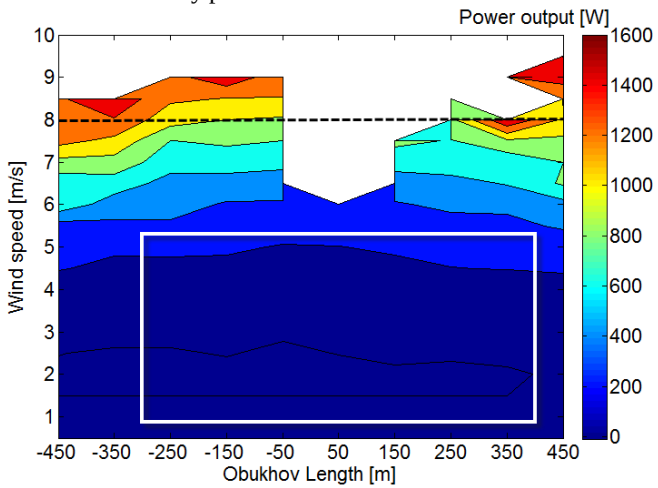

Figure 41 shows a similar analysis, using the 1-min dataset and TI as the turbulence parameter. The undisturbed sector, represented by the white rectangle, goes up to 8 m/s, as already discussed. Above 8 m/s, lower TI levels indicate an improved SWT performance. The relation between TI and stability is plausible, once a low TI can be related with a downward net heat flux in the stable atmosphere, which consumes the mechanically generated turbulence. Contrariwise, higher TI levels are analogous to unstable conditions, with both mechanical and thermal generation components in action.

Figure 41 – 1-min TI power 2D surface

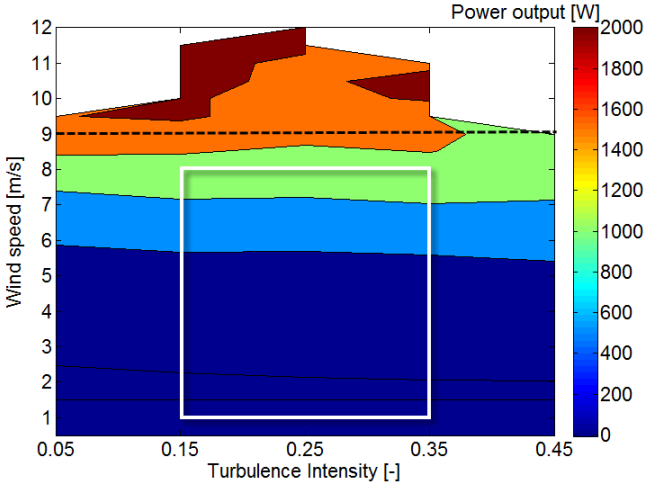

The power surface approach unites the turbulence parameters in order to illustrate the power collection dependence as a multi-variable relation. This work aimed to provide more inputs towards a holistic SWT power performance assessment, with new tools that are not explicitly stated in the current standard procedures. Results indicate that a hybrid assessment, with TI and L as classification parameters, and a power surface approach to data representation are promising.

5 FINAL REMARKS

The present work aimed to identify the most favorable and adverse turbulence conditions for small wind generation trough a case study. Obukhov length (L) and turbulence intensity (TI) were used as parameters. Results propose a hybrid approach for SWT power performance, with both a statistical analysis with TI and a physical view into the atmospheric stability process with L.

The project of a Wind Energy Experimental Setup resulted in the deployment of a 2.1kW small wind turbine and a 10m meteorological mast, both installed close to a building in the UFSC Campus. Therefore, a grid-tied distributed generation system is currently operating, with delivered electricity to the university laboratories. In addition to energy production, this platform is also being used for educational purposes.

Undergrad students from engineering and meteorology courses already performed technical visits, opening discussions in renewable energies, sustainability and other issues. An extension project with a local high school was also developed, involving the students in basic wind energy topics.

This work shed some light on two central themes. First, a SWT performance assessment that considers the influence of ambient turbulence. Analysis for SWTs so far used turbulence intensity (TI) as a classification parameter. An approach based on atmospheric stability was brought from large wind turbine studies and applied in this case study, resulting in an assessment procedure with TI and atmospheric stability as two complementary criteria.

The second issue addressed by this study is the concept of a one-dimensional power curve. Since the influence of turbulence is already a common sense, it's natural to suggest a way to include this parameter in the power curve specification. Although normalization can be performed, limitations for turbulence as a statistical parameter may be included. In this sense, this work presents an approach based on power surfaces, with deviations in power collection caused both by TI and Obukhov length (stability) parameters.

5.1 CONCLUSIONS

This work presents a stability-dependent and TI-dependent small wind turbine performance assessment, using both the Obukhov length and turbulence intensity as classification criteria. Based on data obtained from a well-instrumented experimental setup, site-specific power curves

and power surfaces clarified the relation between SWT power collection and turbulence. The main conclusions can be stated as:

- When dealing with complex terrain and high ambient turbulence, statistical data filtering and a sector analysis for meteorological variables and flux measurements are essential, in order to validate the experimental data with the basic assumptions involving power curves and atmospheric stability calculations;
- At low wind speeds, in the maximum power tracking region, high turbulence levels increase power collection. Turbulence intensity describes well the behavior in this power curve region.
- Close to the rated wind speed, the SWT presents a decreasing tendency in power collection. Turbine control aspects may be involved in the presented results. Atmospheric stability, trough Obukhov length, could spot this underperformance in unstable conditions;
- Presented results are in agreement with those obtained in previous studies based on turbulence intensity, though clarifying the decreasing power collection phenomena close to rated wind speeds with a physical explanation with Obukhov length parameter;
- Results indicate a consistent power collection dependence on stability conditions. With a statistical nature, turbulence intensity parameter presents limitations in relation to explaining the measured pattern. For atmospheric stability-dependent power curves, measured deviations between stable and unstable conditions go up to 51%.
- Atmospheric stability was an appropriate approach to evidence the decreasing tendency in power output at higher speeds (knee power curve region). Obukhov length (L) was found to be an appropriate stability parameter and should be used along with TI as turbulence classification criteria, as a hybrid (physical and statistical) power performance assessment.
- The work presents a multi-variable representation, with the use of power surfaces. 3D and 2D surfaces were better ways to represent the correlation between wind, power output and turbulence, avoiding the normalization with a single value for turbulence. Undisturbed regions within the power surface can still be represented as usual power curves.

- The proposed SWT power performance approach along with power surface usage can lead to safer and viable small wind applications in complex terrain. Therefore, the works give a better comprehension of small wind generation barriers in urban environments and other complex terrains
- Successful SWT grid-tied systems rely on more elaborated turbine tests and a better description of atmospheric conditions at the site, hence the use of the procedure described herein is recommended.

5.2 FURTHER STUDIES

The experimental setup is fully operational, collecting data and generating electricity for university labs. Therefore, a wide range of further studies can be performed. Also, this case study has the potential to accomplish more educational purposes, with more extension and research projects.

A first suggestion is related with flux measurements filtering and validation. Another 10m met mast for eddy covariance is installed 60m away from the experimental setup. Therefore, there is a possibility for data validation with a better empirical reference that suffers less obstacle influence. Moreover, the study should go deeper in the 20 Hz data filtering with EddyPro, with further sensitivity and sector analysis. The installed meteorological station can also be improved with radiation measurements as well as sensors for latent heat flux estimation, in order to increase the eddy covariance accuracy.

An important aspect of power performance is the SWT control strategy. Measurements of rotor RPM and other parameters can supply evidence for the control limitations of wind turbines. Another common topic discussed in small wind application, and measured in certification schemes, is the acoustic noise levels. Field measurements at different distances from the hub at various wind regimes can validate or disprove the manufacturer emission noise map (WINDTEST, 2009) for urban environment applications.

The experimental setup is part of a larger R&D project, focused on short-term wind power forecasting. One of the measurement equipment is a 500m Windcube8® LiDAR wind profiler, that is going to come into an annual maintenance and calibration at the same site of the experimental setup. A measurement campaign with this wind profiler will enable a validation of the atmospheric stability assumptions considered in the present work.

Averaged wind profiles could then be correlated with universal similarity functions, based on the presented flux measurements. Remote sensing for wind energy applications are already a tendency, with increasing acceptance as reference wind measurements for resource and power performance assessment.

RESUMO EXPANDIDO

1. INTRODUÇÃO E OBJETIVOS

Pequenos aerogeradores mostram-se como uma solução real para aplicações de geração distribuída, podendo ser considerados potenciais protagonistas em futuros sistemas *smart grid* (WWEA, 2012). Em 2012, a Agência Brasileira de Energia Elétrica avançou com a regulamentação no Brasil do sistema de compensação de energia para agentes de microgeração distribuída, por fontes renováveis, com até 1MW de potência instalada (ANEEL, 2012a).

Jutamente com suas vantagens, as aplicações de microgeração eólica encontram desafios. Quando instalados em zonas urbanas, próximos ao consumidor final, pequenos aerogeradores estão sujeitos a altos níveis de turbulência atmosférica, influenciada pela elevada complexidade do terreno.

Este cenário mostra, portanto, a necessidade de uma melhor compreensão do regime de ventos em terrenos complexos, bem como a descrição do comportamento do aerogerador sob tais circustâncias. O perfil de velocidade do vento é geralmente descrito com funções exponenciais ou logarítmicas, que estão restritas a terrenos planos e condições atmosféricas muito específicas (ARYA, 2001).

A variação do perfil de vento em função da estabilidade atmosférica já é conhecida (STULL, 1988) com estudos que apresentam o impacto na produção de energia para aerogeradores com elevada área varrida pelo rotor (WHARTON; LUNDQUIST, 2012). No contexto de pequenos aerogeradores em terreno complexo, barreiras técnias também são encontradas na descrição dos aspectos de turbulência e previsão do potencial eólico (SMITH et al., 2012).

Baseando-se nos resultados já obtidos em parques eólicos (WHARTON; LUNDQUIST, 2010), o presente trabalho busca avaliar a hipótese da influência da estabilidade atmosférica no desempenho de um pequeno aerogerador. Um aparato experimental terá como objetivo a caracterização da estabilidade atmosférica em um terreno complexo, onde os resultados serão correlacionados com a geração de um pequeno aerogerador instalado em campo.

Para tanto, a seguinte pergunta de pesquisa é formulada: Qual o impacto da estabilidade atmosférica no desempenho de um pequeno aerogerador em terreno complexo e como avaliá-lo?

Tem-se, portanto, como objetivo geral:

- Avaliar o impacto da estabilidade atmosférica no desempenho de um pequeno aerogerador em terreno complexo.

O objetivo geral dessobra-se nos seguintes objetivos específicos:

- Compreender a influência da estabilidade atmosférica na extração de energia cinética do vento por um aerogerador;
- Projetar e construir uma plataforma experimental com um pequeno aerogerador e uma torre anemométrica, com medições de vento, potência gerada e fluxos turbulentos;
- Caracterizar a estabilidade atmosférica, intensidade de turbulência e parâmetros de desempenho do pequeno aerogerador;
- Correlacionar estabilidade atmosférica e intensidade de turbulência com a geração do pequeno aerogerador;
- Desenvolver um procedimento para avaliação de performance de um pequeno aerogerador baseado na estabilidade atmosférica.

O capítulo 2 apresenta aspectos relacionados à energia eólica e micrometeorologia, que são considerados os dois pilares teóricos do trabalho. No capítulo 3 é descrita a metodologia, com o aparato experimental desenvolvido bem como as ferramentas utilizadas para o processamento e análise dos dados. O capítulo 4 abrange os resultados obtidos para as medições de regime do vento, operação do AG e curvas de potência. No capítulo 5 são listadas as principais conclusões, bem como algumas perspectivas de uso dos equipamentos instalados e recomendações para futuros trabalhos.

2. MATERIAIS E MÉTODOS

Para este estudo de caso foi desenvolvida a Plataforma Experimental em Energia Eólica (Fig. 12), localizada no Campus Sul da Ilha da UFSC e instalada junto ao prédio do Núcleo Ressacada de Pesquisas em Meio Ambiente (REMA). Esta plataforma experimental é composta por uma torre anemométrica, em operação desde Novembro de 2012, bem como um pequeno aerogerador, que gera energia para os laboratórios da universidade desde Janeiro de 2013.

Com base em análises prévias (SANTOS, 2011), o pequeno aerogerador Skystream 3.7 foi selecionado para o estudo. A tabela 2 apresenta suas especificações técnicas. Dificuldades foram enfrentadas na instalação, na tentativa de integrar o aerogerador ao prédio. Após a constatação de ruído excessivo e risco de danos à estrutura do prédio, optou-se pela construção de uma fundação de concreto independente, a 3m de distância do prédio, com uma torre estaiada com 19m de altura. O

apêndice A1 apresenta o logbook do experimento, com os principais acontecimentos e observações.

A torre anemométrica foi instalada no telhado do mesmo prédio a uma altura de 18m. Os instrumentos instalados permitem a coleta de dados de velocidade e direção do vento, temperatura e umidade relativa e pressão atmosférica. Também foi instalado um anemômetro sônico 3D, capaz de medir em alta frequência as componentes tridimensionais do vento. Um transdutor de potência foi integrado ao sistema de medição para registrar com precisão os dados de produção de energia do AG. A tabela 3 apresenta detalhes da instrumentação. O apêndice A2 mostra as especificações de cada equipamento instalado.

Com a análise do layout do experimento (Fig. 14), podemos observar que os equipamentos estão sob influência do prédio e da vegatação que o cerca. Contudo, o experimento localiza-se em uma fazenda, com terreno relativamente plano no entorno. Portanto, torna-se possível a realização de medições de fluxo turbulento com a avaliação de um terreno complexo. O apêndice A4 apresenta uma visão 360º do local.

Todos os dados são monitorados em tempo real e coletados através de um datalogger, conectado diretamente à rede da universidade. O apêndice A3 detalha os metadados do experimento, com todas as variáveis e parâmetros medidos. Um algoritmo de filtragem de dados é aplicado à série histórica, com aplicação de flags que indicam a qualidade do dado em questão (Fig. 15).

A utilização de um anemômetro sônico 3D permite o cálculo das perturbações turbulentas em cada componente de velocidade. A covariância destas perturbações, chamadas de fluxos turbulentos, fornecerá parâmetros quantitativos para avaliar o transporte de momento e calor ao longo da camada limite superficial.

O software EddyPRO® é utilizado para o processamento e filtragem dos dados de fluxos turbulentos. Diversas análises e filtros são aplicados com objetivo de indicar quais os dados válidos com as premissas do método eddy covariance. A tabela 5 mostra as configurações utilizadas no software para o presente estudo.

Para estimativa da estabilidade atmosférica, a Teoria de Similaridade de Monin-Obukhov (MOST) é invocada. Logo, o comprimento de Obukhov (L) será utilizado como parâmetro de avaliação da estabilidade. Uma classificação com três condições de estabilidade (instável, neutra e estável) foi desenvolvida para o estudo de caso. A tabela 6 apresenta as faixas de L para cada uma das três condições de estabilidade atmosférica.

3. RESULTADOS E DISCUSSÃO

A Plataforma Experimental em Energia Eólica da UFSC está em pleno funcionamento e necessita apenas de manutenção preventiva. Os resultados estão sendo coletados e armazenados continuamente, com um banco de dados que já somam mais de 15.217 horas de dados válidos entre Novembro de 2012 e Agosto de 2013, o que representa uma taxa de recuperação de 98,84%.

Com mais de um ano de dados coletados, torna-se possível uma avaliação do regime de ventos no local. Os resultados do anemômetro sônico 3D foram comparados ao anemômetro de copo, com objetivo de validar as medições. As distribuições de Weibull de ambos os instrumentos concordam entre si (Fig. 17).

Com relação à direção do vento, apesar da comparação entre a rosa dos ventos do wind vane e do sônico 3D concordarem na média (Fig. 18), foi verificada a possibilidade da influência do prédio e da vegatação nas medições. Uma análise setorial foi realizada e apresentou desvios entre os ventos provenientes do norte e do sul (Fig. 20). Portanto, observa-se regimes de vento distintos em função da direção do vento, evidenciando uma influência do prédio sobre as medições.

Pelo fato do AG ter entrado em pleno funcionamento apenas em Dezembro de 2013, o período de análise escolhido para análise consiste em seis meses de dados, entre Dezembro de 2013 e Maio de 2014. Para este período, foram filtrados dados para construção da curva de potência do AG bem como para o cálculo dos fluxos turbulentos e, consequentemente, do comprimento de Obukhov (L).

No presente trabalho observou-se uma performance 13,6% maior do AG (Fig. 30), quando sua curva de potência foi comparada com a do fabricante (WINDTEST, 2009). A média de TI do local é de 32%, contra 9% no certificado do fabricante. Pelo fato de não terem sido registradas velocidades acima de 9 m/s, a elevada turbulência atmosférica pode ter influenciado uma melhoria na performance. O parâmetro TI, portanto, tende a caracterizar o comportamento da curva de potência a baixas velocidades.

O cálculo do comprimento de Obukhov para este estudo de caso mostrou um comportamento esperado, com condições instáveis durante o dia e uma atmosfera predominantemente estável a noite (Fig. 33). Com estes resultados, foi possível construir curvas de potência específicas para cada condição de estabilidade. O parâmetro intensidade de turbulência também foi utilizado para construção de curvas específicas.

Ao comparar as curvas de potência por estabilidade atmosférica e por intensidade de turbulência, observa-se que desvios em relação ao comportamento médio iniciam a partir de 8 m/s (Fig. 34), ou seja, na região mais próxima à velocidade nominal (11 m/s). Para esta região, o comprimento de Obukhov conseguiu evidenciar que a queda de potência ocorre em condiçõe de atmosfera instável. A intensidade de turbulência não obteve sucesso em evidenciar tal comportamento, devido principalmente a sua natureza estatística.

Os resultados apresentados neste trabalho apontam para uma análise de desempenho que utiliza dois parâmetros para análise. Em baixas velocidades, a intensidade de turbulência foi capaz de caracterizar o aumento na produção do AG em um terreno complexo. Para velocidades próximas da velocidade nominal, o comprimento de Obukhov evidencia a queda de potência gerada. Portanto, os dois parâmetros mostraram-se complementares e devem ser utilizados em conjunto.

Com a comprovação de influência da turbulência no desempenho do pequeno aerogerador, é proposta também uma nova representação para curva de potência. Para além de uma representação bidimensional, apresenta-se o conceito de uma superfície de potência, capaz de representar a relação entre velocidade, potência gerada e turbulência (Figs. 38, 39, 40 e 41).

4. CONCLUSÕES

O presente trabalho apresenta a influência da estabilidade atmosférica no desempenho de um pequeno aerogerador em terreno complexo. Os resultados propõem uma análise de desempenho que utiliza o comprimento de Obukhov (L) e a intensidade de turbulência (TI) como parâmetros de análise.

Dois aspectos fundamentais são esclarecidos no trabalho. O primeiro está relacionado com a influência da turbulência no desempenho do AG. Estudos recentes com pequenos aerogeradores limitaram-se à utilização da intensidade de turbulência como parâmetro de análise. Devido a sua natureza estatística, são observadas limitações na descrição do comportamento do AG próximo da região de potência nominal. A estabilidade atmosférica, através do comprimento de Obukhov, mostrou-se um parâmetro complementar, evidenciando a queda de potência próximo à potência nominal.

O segundo aspecto está relacionado à representação da curva de potência. Dada a influência da turbulência, uma superfície de potência mostrou-se uma ferramenta adequada para representar o desempenho do

equipamento, ao relacionar velocidade, potência e turbulência. Com esta abordagem multidimensional, possíveis limitações impostas por uma normalização, como realizada com o parâmetro de densidade do ar, podem ser superadas.

A plataforma experimental também foi utilizada para fins educativos, bem como para extensão universitária. Alunos de graduação de Engenharia e Meteorologia realizaram visitas técnicas aos equipamentos, com discussões sobre energias renováveis e sustentabilidade. Um projeto de divulgação científica também foi realizado, envolvendo alunos do ensino médio de uma escola pública da região.

Aplicações de geração eólica distribuída mais confiáveis e seguras dependem de testes e análises de desempenho mais elaboradas, que descrevam com mais detalhe a influência das condições atmosféricas no potencial de produção do AG. Sugere-se, portanto, a utilização do procedimento apresentado.

REFERENCES

ANEEL. **Resolução Normativa 482 de 17/04/2012**Brasilia, BrazilAgencia Nacional de Energia Eletrica, , 2012a.

ANEEL. **Resolução Normativa 517 de 11/12/2012**Brasilia, BrazilAgencia Nacional de Energia Eletrica, , 2012b.

ANEEL. **Micro e minigeração distribuída: sistema de compensação de energia elétrica (Cadernos Temáticos ANEEL)**Brasilia, BrazilANEEL, , 2014. Disponível em: <http://www.aneel.gov.br/biblioteca/downloads/livros/caderno-tematico-microeminigeracao.pdf>

ARYA, S. P. **Introduction to Micrometeorology**. 2nd. ed. London: Academic Press, 2001. v. 79

AUBINET, M.; VESALA, T.; PAPALE, D. **Eddy Covariance: A Practical Guide to Measurement and Data Analysis**. London: Springer, 2012.

BURTON, T.; SHARPE, D.; JENKINS, N.; BOSSANYI, E. **Wind Energy Handbook**. Chichester: John Wiley & Sons, 2001.

CARPMAN, N. **Turbulence Intensity in Complex Environments and its Influence on Small Wind Turbines**. Uppsalla: Dept. of Earth Sciences, Uppsalla University, 2010.

CELESC. **Requisitos para a conexão de micro ou mini geradores de energia ao sistema elétrico da Celesc Ditribuição** Florianopolis, BrazilCELESC, , 2013.

DAMAS, L. B.; SANTOS, P. A. A.; MORESCO, G. M.; PASSOS, J. C. Cenario Nacional e Tendências para geração eólica. **ABCM Engenharia**, v. 17, n. 1, p. 14, 2012.

DAMAS, L. B. **Análise de geração e aplicação do método MCP em dois parques eólicos em operação no Brasil.** [s.l.] (Dissertação de Mestrado) Engenharia Mecanica - Universidade Federal de Santa Catarina, 2013.

ELLIOTT, D. L.; CADOGAN, J. B. Effects of wind shear and turbulence on wind turbine power curves. **Wind Energy**, p. 10-14, set. 1990.

ENCRAFT. **Warwick Wind Trials: FInal Report**. [s.l.] Encraft, 2008. Disponível em: <http://www.warwickwindtrials.org.uk/resources/Warwick+Wind+Trials+Final+Report+.pdf>.

EPE. **Balanço Energetico Nacional 2013: Ano Base 2012**. Rio de Janeiro: Empresa de Pesquisa Energetica, 2013.

FOKEN, T. 50 Years of the Monin–Obukhov Similarity Theory. **Boundary-Layer Meteorology**, v. 119, n. 3, p. 431-447, 2006.

FOKEN, T.; NAPPO, C. J. **Micrometeorology**. [s.l.] Springer, 2008.

GARRATT, J. R. Review of Drag Coefficients over Oceans and Continents. **Monthly Weather Review**, v. 105, n. 7, p. 915-929, 1977.

GOTTSCHALL, J.; PEINKE, J. How to improve the estimation of power curves for wind turbines. **Environmental Research Letters**, v. 3, n. 1, p. 015005, 2008.

GWEC. **Global Wind Energy Outlook 2012**. Brussels: Global Wind Energy Council, 2012.

HAU, E. **Wind Turbines. Fundamentals, Technologies, Application, Economics**. 2nd. ed. New York: Springer, 2006.

HENNESSEY, J. P. JR. Some Aspects of Wind Power Statistics. **Journal of Applied Meteorology**, v. 16, p. 119-128, fev. 1977.

IEA. **Energy Technology Perspectives 2014:** Paris: International Energy Agency, maio 2014.

IEC. **Wind turbines, part 12-1: power performance measurements of electricity producing wind turbines**Geneva, SwitzerlandInternational Electrotechnical Commission, , 2005.

IEC. **Wind turbines, part 2: design requirements for small wind turbines**Geneva, SwitzerlandInternational Electrotechnical Commission, , 2013.

LANGE, M.; FOCKEN, U. **Physical Approach to Short-Term Wind Power Prediction**. Berlin: Springer, 2006.

LEDO, L.; KOSASIH, P. B.; COOPER, P. Roof mounting site analysis for micro-wind turbines. **Renewable Energy**, v. 36, n. 5, p. 1379-1391, 2011.

LEE, X.; MASSMAN, W. J.; LAW, B. **Handbook of Micrometeorology: A Guide for Surface Flux Measurement and Analysis**. [s.l.] Springer, 2004.

LI-COR. **EddyPro® 4.2 Help and User's Guide**. Lincoln, NE: LI-COR, Inc, 2013.

LUBITZ, W. D. Impact of ambient turbulence on performance of a small wind turbine. **Renewable Energy**, v. 61, n. 0, p. 69-73, 2014.

MATHIEU, J.; SCOTT, J. **An Introduction to Turbulent Flow**. [s.l.] Cambridge Univeristy Press, 2000.

MEASNET. **Power performance measurement procedure, version 5**Measuring Network of Wind Energy Institutes, , 2009a.

MEASNET. **Evaluation of site-specific wind conditions, version 1**Measuring Network of Wind Energy Institutes, , 2009b.

MELLINGHOFF, H. **Development of power curve measurement standards**. [s.l.] DEWI GmbH, 2013. Disponível em: <http://www.dewi.de/dewi_res/fileadmin/pdf/publications/Publikations/S14_4_Mellinghoff.pdf>.

MERTENS, S. **Wind energy in the built environment**. Netherlands: TU Delft, 2006.

MONIN, A. S.; OBUKHOV, A. M. Basic laws of turbulent mixing in the atmosphere near the ground. **Tr. Akad. Nauk., SSSR Geophiz. Inst.**, n. 24 (151), p. 163-187, 1954.

OKE, T. R. **Boundary Layer Climates**. New York: Halsted, 1987.

PEÑA, A.; HAHMANN, A. N. Atmospheric stability and turbulence fluxes at Horns Rev—an intercomparison of sonic, bulk and WRF model data. **Wind Energy**, v. 15, n. 5, p. 717-731, 2012.

SANTOS, P. A. A. **Análise de investimento e desempenho de um pequeno aerogerador instalado em zona urbana**. Florianopolis: (Trabalho de Conclusao de Curso) Engenharia de Producao e Sistemas - Universidade Federal de Santa Catarina, 2011.

SANTOS, P. A. A.; DAMAS, L. B.; MORESCO, G. M.; PASSOS, J. C. **Análise de investimento e desempenho de um pequeno aerogerador instalado em zona urbana**Anais...Sao Paulo: Instituto Acende Brasil, 2011

SATHE, A.; GRYNING, S.-E.; PEÑA, A. Comparison of the atmospheric stability and wind profiles at two wind farm sites over a long marine fetch in the North Sea. **Wind Energy**, v. 14, n. 6, p. 767-780, 2011.

SMITH, J.; FORSYTH, T.; SINCLAIR, K.; OTERI, F. **Built-Environment Wind Turbine Roadmap**. Golden, CO: National Renewable Energy Laboratory (NREL), 2012.

STANKOVIC, S.; CAMPBELL, N.; HARRIES, A. **Urban Wind Energy**. London: Earthscan, 2009.

STULL, R. B. **An Introduction to Boundary Layer Meteorology**. [s.l.] Springer Netherlands, 1988.

SUNDERLAND, K.; WOOLMINGTON, T.; BLACKLEDGE, J.; CONLON, M. Small wind turbines in turbulent (urban) environments: A consideration of normal and Weibull distributions for power prediction. **Journal of Wind Engineering and Industrial Aerodynamics**, v. 121, n. 0, p. 70-81, 2013.

VICKERS, D.; MAHRT, L. Quality Control and Flux Sampling Problems for Tower and Aircraft Data. **Journal of Atmospheric and Oceanic Technology**, v. 14, p. 512-526, 1997.

WAGNER, R.; COURTNEY, M.; GOTTSCHALL, J.; LINDELÖW-MARSDEN, P. Accounting for the speed shear in wind turbine power performance measurement. **Wind Energy**, v. 14, n. 8, p. 993-1004, 2011.

WAGNER, R.; COURTNEY, M. **Accounting for the speed shear in wind turbine power performance measurement**. [s.l.] Risø National Laboratory for Sustainable Energy, 2010.

WALLACE, J. M.; HOBBS, P. V. **Atmospheric Science: An Introductory Survey**. Oxford: Elsevier, 2006.

WHARTON, S.; LUNDQUIST, J. K. **Atmospheric Stability Impacts on Power Curves of Tall Wind Turbines – An Analysis of a West Coast North American Wind Farm**. Livermore, CA: Lawrence Livermore National Lab, 2010.

WHARTON, S.; LUNDQUIST, J. K. Assessing atmospheric stability and its impacts on rotor-disk wind characteristics at an onshore wind farm. **Wind Energy**, v. 15, n. 4, p. 525-546, 2012.

WINDTEST. **Power performance measurement of the Skystream 3.7 at Kaiser-Wilhelm-Koog, Germany according to IEC 61400-12-1 and BWEA**. [s.l.] WINDTEST Kaiser-Wilhelm-Koog GmbH, nov. 2009.

WOOD, D. **Small Wind Turbines: Analysis, Design and Application**. London: Springer, 2011.

WWEA. **Small Wind World Report**. Bonn, Germany: World Wind Energy Association, 2012.

APPENDIX A: EXPERIMENTAL SETUP DETAILS

APPENDIX A1: EXPERIMENTAL SETUP LOGBOOK

Date (yyyy-mm-dd)	Local Time (GMT-3)	Equipment	Notes
2012-11-28	12:10:00	Tower	Operation starts. Configuration CRBasic script Version 4 (Config V4).
2013-01-13	18:00:00	SWT	Installation of SWT next to the building.
2013-02-21	12:20:00	Tower	Datalogger repeated one hour of data. Typical failure with no abnormal operation
2013-03-07	11:50:00	Tower	3D sonic anemometer installation. Change to Config V5. Tower deactivated and no data from 2013-03-06 13:10:00 to 2013-03-07 11:40:00
2013-03-08	15:00:00	Tower	Atmospheric discharge protection system installation. Invalid data from 15:00:00 to 17:10:00
2013-03-08	19:00:00	SWT	Decomissionament of old tower and SWT installation in a new tower, with thicker walls. The same installation procedure was conduced.
2013-03-13	09:10:00	Tower	Change to Config V6. Covariance calculation problem. No data at 09:00:00
2013-03-13	15:00:00	SWT	The wrong assembly tilts the current tower. SWT does not generate with the stronger northern winds. Skyview data showed this obvious trend. Hence, the tower is tilted to the north, making harder from the SWT to gain enough lift for power production. Students and researchers working on the building are also complaining of the noise and vibration in the structure. A power transducer will be installed, and a new solution is needed.
2013-03-15	08:50:00	Tower	Change to Config V7. Covariance calculation problem. No data at 08:40:00

2013-07-10	13:50:00	Tower	Power transducer installation. Change to Config V9. New 60min flux measurement data table. Insertion of four new columns in 10min data table (46 columns). Insertion of mean power and mean wind speed and direction into 1Hz data table. No data from 2013-07-10 14:00:00 to 2013-07-10 15:20:00
2013-08-28	15:10:00	Tower	Change to Config V10. Skip scan correction w/ measurement resolution.
2013-12-10	15:30:00	SWT	After construction of an independent foundation, the SWT was relocated 3m apart from the building. The same tower is been used, but now with two stages of guy wires, each one with 3 points (120^{o} apart). Tower was aligned with a theodolite.
2013-12-17	12:00:00	SWT	Wind speeds around 6 m/s from ESE and SE sectors. Wind speed is sufficiently high, but direction varies a lot and turbine can't align with the wind and start operation. After some data analysis, other similar occasions happen, like the two previous days of this observation.
2013-12-27	12:30:00	SWT	With data analysis, it was observed the same underperformance behavior in medium intensity (5 m/s) SE winds. Guy wires are constantly fastened, but maybe there's a tower misalignment
2014-01-17	14:00:00	SWT	Realignment was realized by the topography team, in order to verify the behavior under ESE and SE winds.
2014-03-29	14:15:00	Tower	Battery voltage is presenting an abnormal behavior since 2013-03-27, indicating a failure in the energy supply system. Urgent need to check solar panel cables and charge controller on field.
2014-04-01	15:00:00	Tower	Charge controller failure due to invasion of ants inside the battery cover. Controller was replaced by spare one (S/N 13290274). Battery cover was cleaned and poison was applied. Desiccant was also replaced.

APPENDIX A2: EQUIPMENT SPECIFICATION

First Class Cup Anemometer	
Make/Model	Thies, P6101H, Class S0.5
Serial Number	03127893
Range	0.3 to 50 m/s
Accuracy	1% of meas. value
Calibration Date	March 21st, 2012
3D Ultrasonic Anemometer	
Make/Model	RM Young, 81000
Serial Number	3716
Range	-50 to 50 m/s, -50 to 50 ^{o}C
Accuracy	±0.05 m/s, ±2 ^{o}C
Calibration Date	October 30th, 2012
First Class Wind Vane	
Make/Model	Thies, P6200H
Serial Number	03121209
Range	0 to 360^{o} without north gap
Accuracy	± 1^{o}
Power transducer	
Make/Model	OHIO Semitronics, PC5-119C
Serial Number	13040547
Range	0 to 5kW
Accuracy	± 0.5% F.S.
Calibration Date	April 15th, 2013
2D Inclinometer	
Make/Model	HL Planartechnik, NS-5/DMG2-I
Serial Number	0838688
Range	- 5^{o} to +5^{o}
Accuracy	±0.03^{o}
Calibration Date	August 3rd, 2011
Datalogger with Ethernet and 2GB memory	
Make/Model	Campbell, CR1000 w/ NL115
Serial Number	47245, 9152
Hygrothermal sensor	
Make/Model	Thies P6312P
Serial Number	95795
Range	-30 to 70 ^{o}C, 0 to 100% r.H.
Accuracy	± 0.2 K, ± 2% r.H.

Barometer	
Make/Model	Thies, P6330.2
Serial Number	S007632
Range	800 to 1100 hPa
Accuracy	±3 hPa
GSM/GPRS Modem	
Make/Model	Duodigit, MC55iT-BR
Serial Number	120607555
GPS	
Make/Model	Garmin, 16x
Serial Number	1A4099935
Solar Panel	
Make/Model	Kyocera Solar, KS20T
Serial Number	33339, 33380, 33453
Max Power	20W @ 1000 W/m^2
Charge Controller	
Make/Model	Morningstar, SHS 10
Serial Number	13290274
Power and Current	170W, 10A

APPENDIX A3: MEASUREMENTS METADATA

AERO_10min Datatable

Scan Frequency: 1Hz | Comma-separated DAT File | Output interval: 10min

#	Colum	Variable	Unity	Format
1	TIMESTAMP	"yyyy-mm-dd HH:MM:SS"	---	---
2	RECORD	Data logger output counter	---	---
3	Vel_10m_WVc(1)	Cup scalar velocity	m/s	FP – 2 bytes
4	Vel_10m_WVc(2)	Cup vector velocity	m/s	FP – 2 bytes
5	Vel_10m_WVc(3)	Wind vane direction	^{o}	FP – 2 bytes
6	Vel_10m_WVc(4)	Wind direction standard deviation	^{o}	FP – 2 bytes
7	Vel_10m_Std	Velocity standard deviation	m/s	FP – 2 bytes
8	Vel_10m_Max	Velocity maximum value	m/s	FP – 2 bytes
9	Vel_10m_SMM	Direction of max velocity	^{o}	FP – 2 bytes
10	VelCubo_Avg	Cubic velocity	m^3/s^3	IEEE – 4 bytes
11	Temp_2m_Avg	Ambient temperature	^{o}C	FP – 2 bytes
12	Umid_2m_Avg	Relative humidity	%	FP – 2 bytes
13	Pressao_Avg	Atmospheric pressure	hPa	FP – 2 bytes
14	Ux_Avg	Crosswind velocity component	m/s	IEEE – 4 bytes
15	Uy_Avg	Alongwind velocity component	m/s	IEEE – 4 bytes
16	Uz_Avg	Vertical velocity component	m/s	IEEE – 4 bytes
17	Ts_Avg	Sonic temperature	K	IEEE – 4 bytes
18	SonicX_WVc(1)	Sonic scalar velocity	m/s	FP – 2 bytes
19	SonicX_WVc(2)	Sonic vector velocity	m/s	FP – 2 bytes
20	SonicX_WVc(3)	Sonic wind direction	^{o}	FP – 2 bytes
21	SonicX_WVc(4)	Sonic wind direction std. dev.	^{o}	FP – 2 bytes

22	Inclinometro_Avg(1)	Sonic boom “x” inclination: W (-), E (+)	^{o}	IEEE – 4 bytes
23	Inclinometro_Avg(2)	Sonic boom “y” inclination: S (-), N (+)	^{o}	IEEE – 4 bytes
24	Inclinometro_Std(1)	“x” inclination std. dev.	^{o}	IEEE – 4 bytes
25	Inclinometro_Std(2)	“y” inclination std. dev.	^{o}	IEEE – 4 bytes
26	rho_a_Avg	Air density	kg/m^3	IEEE – 4 bytes
27	tau	Turbulent shear stress	kg/ms^2	IEEE – 4 bytes
28	u_star	Friction velocity	m/s	IEEE – 4 bytes
29	Hs	Sensible heat flux	W/m^2	IEEE – 4 bytes
30	TKE	Turbulent kinetic energy		IEEE – 4 bytes
31	Cov_Ux_Ux	Turbulent covariance $\overline{u'u'}$	m^2/s^2	IEEE – 4 bytes
32	Cov_Ux_Uy	Turbulent covariance $\overline{u'v'}$	m^2/s^2	IEEE – 4 bytes
33	Cov_Ux_Uz	Turbulent covariance $\overline{u'w'}$	m^2/s^2	IEEE – 4 bytes
34	Cov_Ux_Ts	Turbulent covariance $\overline{u'\theta'}$	mK/s	IEEE – 4 bytes
35	Cov_Uy_Uy	Turbulent covariance $\overline{v'v'}$	m^2/s^2	IEEE – 4 bytes
36	Cov_Uy_Uz	Turbulent covariance $\overline{v'w'}$	m^2/s^2	IEEE – 4 bytes
37	Cov_Uy_Ts	Turbulent covariance $\overline{v'\theta'}$	mK/s	IEEE – 4 bytes
38	Cov_Uz_Uz	Turbulent covariance $\overline{w'w'}$	m^2/s^2	IEEE – 4 bytes
39	Cov_Uz_Ts	Turbulent covariance $\overline{w'\theta'}$	mK/s	IEEE – 4 bytes
40	Cov_Ts_Ts	Turbulent covariance $\overline{\theta'\theta'}$	K^2	IEEE – 4 bytes
41	PTemp_Avg	Datalogger temperature	^{o}C	FP – 2 bytes
42	batt_volt_Avg	Battery setup voltage	V	FP – 2 bytes
43	Potencia_Avg	SWT mean power output	W	IEEE – 4 bytes
44	Potencia_Max	SWT maximum power output	W	IEEE – 4 bytes
45	Potencia_Min	SWT minimum power output	W	IEEE – 4 bytes
46	Potencia_Std	SWT power output std. dev.	W	IEEE – 4 bytes

AERO_20Hz Datatable

Scan Frequency: 20Hz | Comma-separated DAT File | Output interval: 20Hz

#	Colum	Variable	Unity	Format
1	TIMESTAMP	"yyyy-mm-dd HH:MM:SS"	---	---
2	RECORD	Data logger output counter	---	---
3	Ux	Crosswind velocity component	m/s	IEEE – 4 bytes
4	Uy	Alongwind velocity component	m/s	IEEE – 4 bytes
5	Uz	Vertical velocity component	m/s	IEEE – 4 bytes
6	Ts	Sonic temperature	K	IEEE – 4 bytes

INCLI_1s Datatable

Scan Frequency: 1Hz | Comma-separated DAT File | Output interval: 1Hz

#	Colum	Variable	Unity	Format
1	TIMESTAMP	"yyyy-mm-dd HH:MM:SS"	---	---
2	RECORD	Data logger output counter	---	---
3	Inclinometro(1)	Sonic boom "x" inclination: W (-), E (+)	º	FP – 2 bytes
4	Inclinometro(2)	Sonic boom "y" inclination: S (-), N (+)	º	FP – 2 bytes
5	Vel_10m	Cup scalar velocity	m/s	FP – 2 bytes
6	Dir_10m	Wind vane direction	º	FP – 2 bytes
7	Potencia	SWT mean power output	W	IEEE – 4 bytes

APPENDIX A4: EXPERIMENT 360^0 VIEW

NORTH

SOUTH

WEST

EAST

APPENDIX A5: INSTRUMENT HEIGHTS
(above ground level)

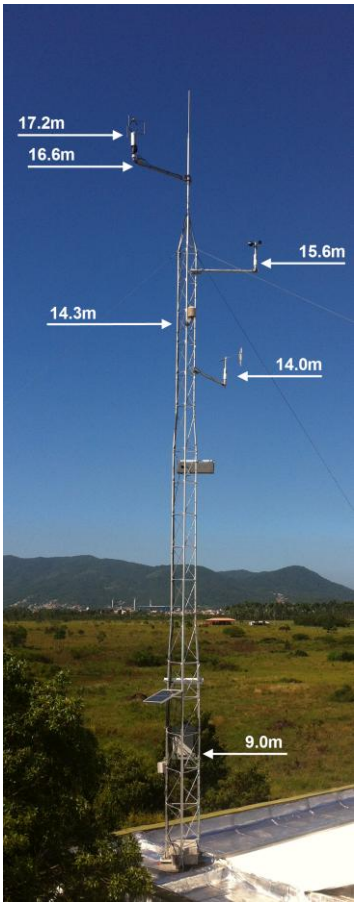

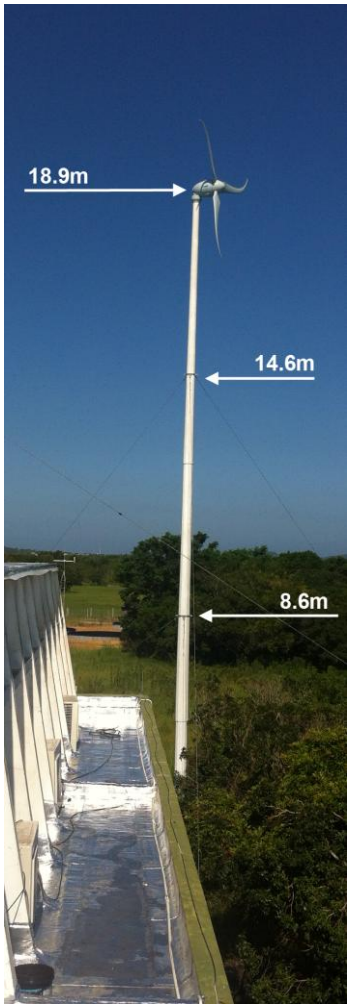

APPENDIX B: MEASUREMENTS TABLE

10-MIN AVERAGE MONTHLY MEASUREMENTS														
		R.R [%]	V_{cup} [m/s]	σ_V [m/s]	TI [%]	σ_{TI} [%]	V_{sonic} [m/s]	θ_{sonic} [K]	Temp [^oC]	R.H. [%]	Pressure [hPa]	Density [kg/m^3]	MEP [kWh]	CF [%]
2012	Dec	100	3.54	0.92	31.3	13.4	-	-	25.4	79.6	1009.5	1.167	-	-
2013	Jan	100	3.32	0.96	33.9	13.4	-	-	24.1	76.5	1012.8	1.177	-	-
	Feb	100	2.95	0.84	33.8	13.5	-	-	25.1	80.6	1011.4	1.170	-	-
	Mar	96.3	2.95	0.90	35.2	13.0	-	-	23.1	82.0	1012.9	1.181	-	-
	Apr	100	2.52	0.73	35.7	14.8	2.64	296.8	22.1	79.5	1015.2	1.189	-	-
	May	100	2.66	0.76	34.9	14.4	2.76	293.8	19.7	80.3	1015.1	1.199	-	-
	Jun	100	2.36	0.74	37.8	15.2	2.52	292.5	18.3	85.8	1016.0	1.206	-	-
	Jul	99.8	2.94	0.87	34.3	13.3	3.00	290.2	16.1	81.2	1018.7	1.220	-	-
	Aug	99.8	3.44	1.01	34.6	13.8	3.53	290.7	16.6	81.0	1017.4	1.216	-	-
	Sep	100	3.07	0.75	26.3	9.4	3.19	293.3	18.6	82.8	1016.0	1.205	-	-
	Oct	97.7	3.42	0.82	25.5	9.0	3.61	295.3	20.5	80.4	1015.5	1.196	-	-
	Nov	93.2	3.98	0.92	25.2	8.9	4.25	297.3	22.2	80.7	1013.4	1.186	-	-
	Dec	98.5	3.21	0.79	25.8	8.8	3.34	299.5	24.2	83.1	1010.0	1.172	56.3	5.3
2014	Jan	90.7	3.20	0.74	24.8	8.5	3.43	301.5	26.0	83.4	1012.0	1.166	102.4	6.6
	Feb	100	3.49	0.80	24.4	8.4	3.75	301.9	26.5	81.0	1012.4	1.165	111.7	7.9
	Mar	100	2.58	0.63	25.7	8.7	2.72	299.6	24.3	84.1	1013.1	1.175	48.4	3.1
	Apr	100	2.74	0.73	27.4	8.9	2.74	297.6	22.5	82.8	1015.5	1.187	60.0	4.0
	May	100	2.52	0.68	27.5	9.7	2.57	294.7	19.8	83.6	1015.5	1.199	50.9	3.3
	Jun	100	2.52	0.64	26.7	9.9	2.68	293.2	18.3	86.7	1016.2	1.207	66.0	4.4
	Jul	100	2.57	0.62	26.0	9.9	2.72	292.6	17.8	84.5	1020.0	1.214	70.5	4.5
	Aug	100	2.95	0.75	26.9	9.4	3.18	292.7	18.0	80.4	1017.4	1.210	104.4	6.7

Ref. density: 1.225 kg/m^3		1-min Measured Power Curve			Stability-dependent			TI-dependent	
Bin	Wind speed	Pout	No. of data sets	Std. uncert.	Pout Stable	Pout Neutral	Pout Unstable	Pout TI<17%	Pout TI>17%
	[m/s]	[W]		[W]	[W]	[W]	[W]	[W]	[W]
4	1.97	-6.5	27358	0.0	-5.2	-3.8	-6.1	-7.7	-6.4
5	2.46	2.1	21926	0.1	6.7	5.9	1.3	3.5	1.9
6	2.96	22.7	18881	0.3	32.8	29.4	17.2	37.4	21.2
7	3.45	92.0	17458	0.4	103.3	116.4	84.8	97.8	91.0
8	3.94	147.1	15779	0.6	158.7	194.8	141.6	156.5	145.1
9	4.43	212.7	13781	0.8	224.9	268.0	209.2	228.3	209.0
10	4.91	297.2	11537	1.1	308.2	364.6	296.0	319.0	291.3
11	5.41	396.3	9600	1.5	405.3	531.7	395.6	420.3	388.5
12	5.89	519.7	7267	2.1	517.1	684.2	524.8	542.1	510.8
13	6.38	665.0	5133	2.9	678.6	846.0	667.7	673.7	660.9
14	6.86	820.8	3249	4.0	837.4	977.1	821.9	836.2	812.8
15	7.35	983.5	1768	6.4	961.8	1206.4	997.8	1010.8	971.4
16	7.84	1195.3	910	10.0	1198.9	1022.3	1200.1	1231.2	1180.0
17	8.35	1350.8	467	16.0	1339.5	-	1378.1	1404.0	1338.2
18	8.85	1553.1	248	24.8	1603.8	-	1536.0	1645.5	1536.7
19	9.34	1617.5	143	34.8	1754.3	-	1555.6	1830.0	1602.7
20	9.85	1813.0	61	54.9	2082.4	-	1568.3	2347.3	1804.1
21	10.34	1896.7	29	89.2	1894.2	-	1624.4	2143.2	1887.6
22	10.80	2105.6	19	78.5	2147.0	-	1708.3	-	2105.6
23	11.36	1937.6	12	149.5	2531.2	-	1534.8	-	1937.6
24	11.88	-	5	-	2508.4	-	-	-	2421.4

Measured 10-min IEC Power Curve							Certified Skystream 3.7 Power Curve					
Bin	Wind speed [m/s]	Power output [W]	Cp [-]	No. of data sets	Std. unc. [W]	TI [%]	Wind speed [m/s]	Power output [W]	Cp [-]	No. of data sets	Std. unc. [W]	TI [%]
4	1.96	-7.0	-0.155	2843	5.6	26	2.02	-17	-0.311	3471	4	8
5	2.46	0.5	0.000	2328	15.8	27	2.51	-12	-0.118	5236	9	8
6	2.95	16.2	0.094	2010	32.2	27	3.00	3	0.017	6353	20	8
7	3.45	41.7	0.156	1831	53.2	26	3.51	34	0.119	6465	31	9
8	3.95	88.9	0.226	1678	71.4	25	4.03	84	0.195	9502	40	9
9	4.42	177.0	0.319	1602	72.2	24	4.46	132	0.226	9778	44	9
10	4.92	243.8	0.324	1369	88.3	23	5.00	203	0.247	6018	55	9
11	5.40	333.8	0.336	1123	109.2	21	5.49	285	0.261	5407	76	9
12	5.89	444.0	0.346	1022	117.6	21	6.00	391	0.275	4924	101	10
13	6.38	583.5	0.359	742	131.4	20	6.50	510	0.282	4619	124	10
14	6.87	731.1	0.362	574	117.3	21	6.99	643	0.285	4570	148	10
15	7.35	894.7	0.362	287	131.7	20	7.49	799	0.288	4194	163	10
16	7.81	1084.7	0.366	125	125.6	20	7.99	968	0.288	3534	173	10
17	8.30	1304.7	0.365	70	130.3	22	8.50	1146	0.284	3093	176	10
18	8.82	1536.6	0.352	28	179.7	27	8.99	1333	0.279	2543	169	10
19	-	-	-	3	-	-	9.48	1531	0.273	1688	171	9
20	-	-	-	1	-	-	9.98	1745	0.267	959	175	9
21	-	-	-	1	-	-	10.47	1938	0.256	553	155	9
22	-	-	-	-	-	-	10.97	2101	0.242	335	152	9
23	-	-	-	-	-	-	11.47	2242	0.226	182	118	10
24	-	-	-	-	-	-	11.93	2301	0.206	105	108	10

APPENDIX C: PUBLISHED ARTICLES

SANTOS, P. A. A.; PASSOS, J. C. Curvas de potência de um pequeno aerogerador em zona de alta turbulência atmosférica. In: **XXII Jornadas de Jóvenes Investigadores**, 2014, Valparaíso.

Curvas de potência de um pequeno aerogerador em zona de alta turbulência atmosférica

Resumo:

O presente trabalho busca avaliar o impacto da turbulência atmosférica no desempenho de um pequeno aerogerador (AG) instalado em terreno complexo. Uma plataforma experimental com um AG de 2.1kW de potência e uma torre anemométrica são utilizados. Operando desde Janeiro/2013 com fornecimento de energia para os laboratórios da Universidade, os resultados caracterizaram o local com alta turbulência atmosférica (média de 32%). Os dados medidos foram classificados em dois níveis de turbulência local, com a construção de curvas de potência por classe de turbulência. Desvios de até 29,5% entre diferentes classes foram observados. Os elevados níveis de turbulência contribuiram para o aumento da geração de energia em baixas velocidades, mas reduzem o desempenho do equipamento a partir de 10,5 m/s. Curvas de potência específicas apontaram as vantagens e limitações desta abordagem. O trabalho contribui com novos fatores para avaliação da microgeração eólica e sugere avanços na metodologia apresentada.

Palavras-chave: Geração distribuída, pequenos aerogeradores, turbulência atmosférica, análise de desempenho, curvas de potência.

SANTOS, P. A. A.; SAKAGAMI, Y.; HAAS, R.; PASSOS, J. C.; TAVES, F. F. Atmospheric stability effects on small wind turbine power collection in a complex terrain. In: **World Renewable Energy Congress XIII**, 2014, London.

Atmospheric stability effects on small wind turbine power collection in a complex terrain

Abstract:

Small wind turbine (SWT) power performance assessment based on atmospheric stability is presented. The experimental setup studied a 2.1kW SWT in a suburban environment with 1 Hz power collection data and 20 Hz turbulent flux measurements. The dataset consists in 4287h of raw data over a six-month period. Measured IEC-based power curve shows an average performance 30% above manufacturer's curve, but with decreasing power output close to rated wind speeds. Results relating power collection increase at low wind speeds with high turbulence levels concur with previous studies. Obukhov length was used as stability parameter, and stability-dependent power curves were compared with the measured average. Above 8 m/s unstable conditions were predominant and evidenced the decreasing power tendency, where turbulence intensity was unable to give consistent results. The paper validates an approach for small wind turbines assessment using a physical parameter as classification criteria, which better explains power collection behavior close to rated conditions.

Keywords: Small wind turbine, Turbulence, Atmospheric stability, Obukhov length.

ATTACHMENT A: SWT PROJECT DOCUMENTATION

SWT TOWER FOUNDATION

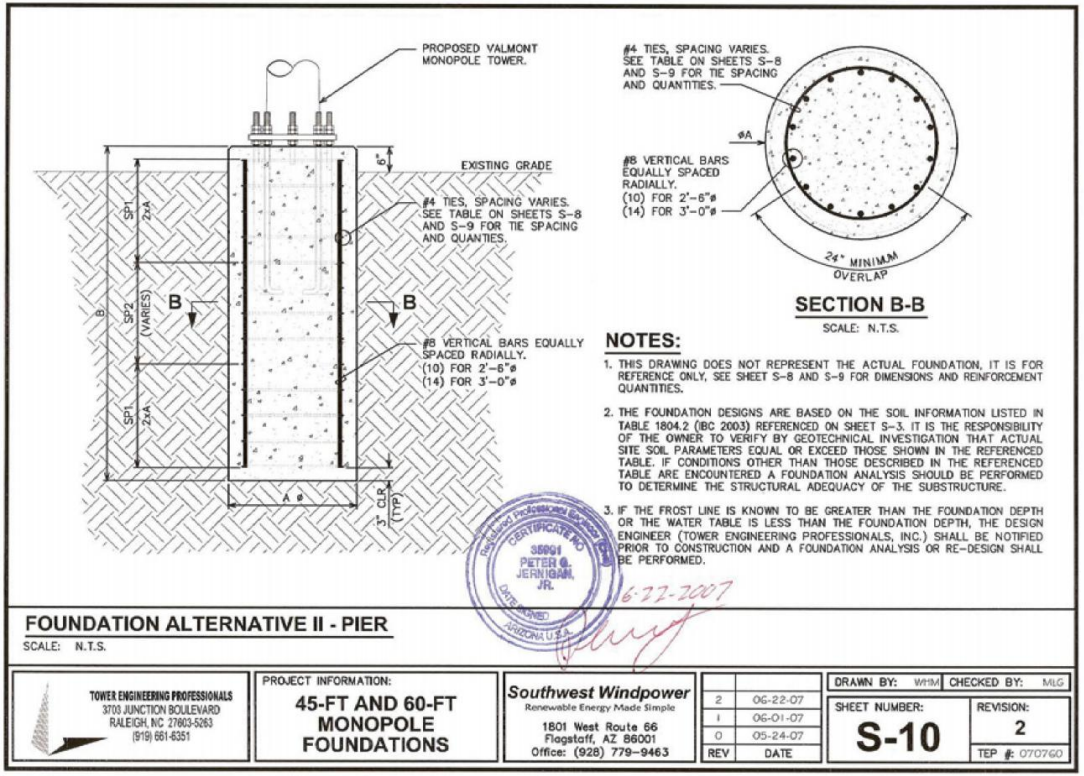

SWT ELECTRICAL DIAGRAM